

A New Solar Radiation Penetration Scheme for Use in Ocean Mixed Layer Studies: An Application to the Black Sea Using a Fine-Resolution Hybrid Coordinate Ocean Model (HYCOM)*

A. BIROL KARA, ALAN J. WALLCRAFT, AND HARLEY E. HURLBURT
Naval Research Laboratory, Oceanography Division, Stennis Space Center, Mississippi

(Manuscript received 1 August 2003, in final form 25 August 2004)

ABSTRACT

A $1/25^\circ \times 1/25^\circ \cos(\text{lat})$ (longitude \times latitude) (≈ 3.2 -km resolution) eddy-resolving Hybrid Coordinate Ocean Model (HYCOM) is introduced for the Black Sea and used to examine the effects of ocean turbidity on upper-ocean circulation features including sea surface height and mixed layer depth (MLD) on annual mean climatological time scales. The model is a primitive equation model with a K -profile parameterization (KPP) mixed layer submodel. It uses a hybrid vertical coordinate that combines the advantages of isopycnal, σ , and z -level coordinates in optimally simulating coastal and open-ocean circulation features. This model approach is applied to the Black Sea for the first time. HYCOM uses a newly developed time-varying solar penetration scheme that treats attenuation as a continuous quantity. This scheme includes two bands of solar radiation penetration, one that is needed in the top 10 m of the water column and another that penetrates to greater depths depending on the turbidity. Thus, it is suitable for any ocean general circulation model that has fine vertical resolution near the surface. With this scheme, the optical depth-dependent attenuation of subsurface heating in HYCOM is given by monthly mean fields for the attenuation of photosynthetically active radiation (k_{PAR}) during 1997–2001. These satellite-based climatological k_{PAR} fields are derived from Sea-Viewing Wide Field-of-View Sensor (SeaWiFS) data for the spectral diffuse attenuation coefficient at 490 nm (k_{490}) and have been processed to have the smoothly varying and continuous coverage necessary for use in the Black Sea model applications. HYCOM simulations are driven by two sets of high-frequency climatological forcing, but no assimilation of ocean data is then used to demonstrate the importance of including spatial and temporal varying attenuation depths for the annual mean prediction of upper-ocean quantities in the Black Sea, which is very turbid ($k_{\text{PAR}} > 0.15 \text{ m}^{-1}$, in general). Results are reported from three model simulations driven by each atmospheric forcing set using different values for the k_{PAR} . A constant solar-attenuation optical depth of ≈ 17 m (clear water assumption), as opposed to using spatially and temporally varying attenuation depths, changes the surface circulation, especially in the eastern Black Sea. Unrealistic sub-mixed layer heating in the former results in weaker stratification at the base of the mixed layer and a deeper MLD than observed. As a result, the deep MLD off Sinop (at around 42.5°N , 35.5°E) weakens the surface currents regardless of the atmospheric forcing used in the model simulations. Using the SeaWiFS-based monthly turbidity climatology gives a shallower MLD with much stronger stratification at the base and much better agreement with observations. Because of the high Black Sea turbidity, the simulation with all solar radiation absorbed at the surface case gives results similar to the simulations using turbidity from SeaWiFS in the annual means, the aspect of the results investigated in this paper.

1. Introduction

The Black Sea is a nearly enclosed region connected to the Sea of Marmara and the Sea of Azov by the narrow Bosphorus and Kerch Straits, respectively (Fig. 1). The importance of the Black Sea extends far beyond

its role as a nearly enclosed sea because it constitutes a unique, nearly land-locked marine environment, and the ventilation of the deep waters is therefore minimal. The Black Sea serves as a small-scale laboratory for investigation of a series of ocean phenomena that are common to different areas of the world ocean. Thus, it is a useful test region in developing a global ocean model.

The most important current feature in the Black Sea is the cyclonic Rim Current located along the upper continental slope (e.g., Sur et al. 1996; Oguz and Besiktepe 1999; Afanasyev et al. 2002). The Rim Current usually follows the topography of the shelf break, and it is accompanied by a series of anticyclonic mesoscale

* Naval Research Laboratory Contribution Number NRL/JA/7320/03/0008.

Corresponding author address: Birol Kara, Naval Research Laboratory, Code 7320, Bldg. 1009, Stennis Space Center, MS 39529–5004.
E-mail: kara@nrlssc.navy.mil

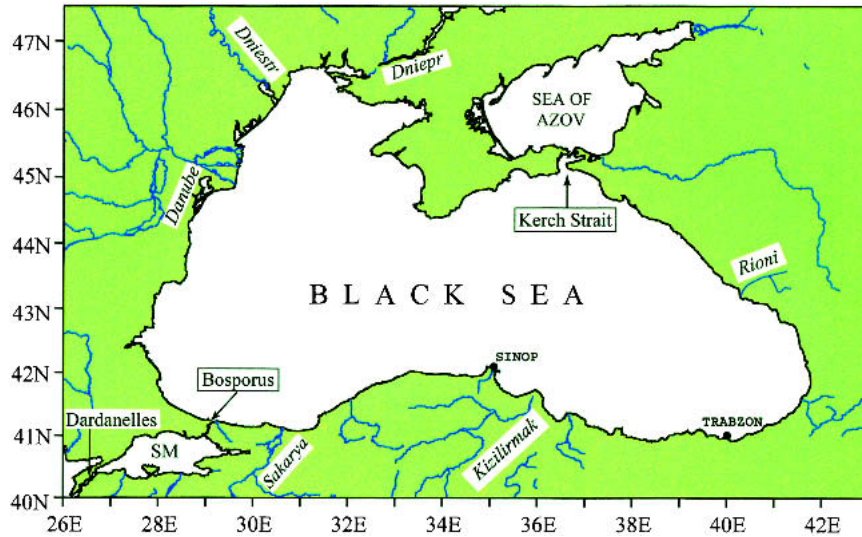


FIG. 1. The geography of the Black Sea. Also shown are rivers discharged into the Black Sea. Only major rivers named on the map are used in the model simulations. Sea of Marmara (SM) is excluded in the model simulations. Two coastal cities (Trabzon and Sinop) used in the text are also marked. The Black Sea presents challenging test areas to study ocean phenomena that are dominated by coastline orientation, coastline shape, and topography.

eddies as well as transient waves with an embedded train of mesoscale eddies propagating cyclonically around the basin. Observational studies (e.g., Oguz et al. 1993; Sur and Ilyin 1997; Afanasyev et al. 2002) and previous Black Sea fine-resolution eddy-resolving ocean general circulation model (OGCM) studies (e.g., Stanev and Beckers 1999; Stanev and Staneva 2000; Staneva et al. 2001) examined upper-ocean quantities, mainly the Rim Current and many semipermanent eddies, using different approaches. None of these OGCM studies, which used the Princeton Ocean Model (POM), Modular Ocean Model (MOM), the Dietrich-Center for Air-Sea Technology (DieCAST) ocean model, or the GeoHydrodynamics Environment Research (GHER) ocean model, directly indicated what turbidity field they used in the mixed layer or how they treated the solar radiation attenuation in the model simulations. Thus, a missing part of previous Black Sea OGCM studies is an examination of upper-ocean features with respect to solar radiation penetrating into and below the mixed layer. Such an examination is necessary for the Black Sea because the sharp density stratification near the surface inhibits the ventilation of subpycnocline waters of the Black Sea, so the euphotic structure is usually confined to the mixed layer, which is directly affected by air-sea interaction processes. Since the region is very biologically active (e.g., Kideys et al. 2000; Oguz et al. 2002), it is necessary for an OGCM to take water turbidity into account even if it is not coupled with a biological model. For example, variations in light-absorbing pigment change the vertical distribution of heating in the mixed layer, thereby affecting upper-ocean dynamics.

Properly including the optical properties of seawater in ocean models is becoming an increasingly important topic as the horizontal and vertical resolution of ocean models increases. In particular, solar penetration plays an important role in numerical ocean model studies (e.g., Schneider et al. 1996). With the availability of a remotely sensed diffuse attenuation coefficient at 490 nm (k_{490}) dataset (McClain et al. 1998), it is now possible to determine the ocean turbidity at high spatial resolution and use it as part of the heat flux forcing in a Black Sea OGCM. By using such a dataset, the time-varying solar penetration schemes (e.g., Morel and Antonie 1994; Nakamoto et al. 2001; Murtugudde et al. 2002; Morel and Maritorea 2001) can treat attenuation as a continuous quantity, which is an improvement over the use of a few discrete attenuation values corresponding to classical Jerlov water types (Jerlov 1976). However, matching attenuation of photosynthetically active radiation (k_{PAR}) to Jerlov water types is needed because the original single decay formulation [e.g., $Q_{sol}(z)/Q_{sol}(0) = 0.49 \exp(-z k_{PAR})$], where $Q_{sol}(z)$ is the remaining (i.e., unabsorbed) solar irradiance (short-wave radiation) at depth z , as used in OGCMs, is only accurate for optical depths deeper than 10 or 20 m (e.g., Murtugudde et al. 2002; Kara et al. 2004; Ohlmann 2003). Unlike ocean models with a bulk mixed layer, which have vertical resolution coarser than 10 m near the surface (e.g., Schneider and Zhu 1998; Schneider et al. 2002; Gildor et al. 2003; Wallcraft et al. 2003), OGCMs that have finer near-surface vertical resolution (e.g., Bleck 2002) often have mixed layer depths (MLDs) much shallower than 10 m and thus need to properly distribute solar radiation within the mixed

layer. A single decay-scale formulation is inadequate for this purpose. Here, a new solar subsurface heating formulation is presented. It still treats attenuation as a continuous quantity (depending only on optical depth and k_{PAR}), but is more accurate (i.e., closer to Jerlov curves from the surface downward for representative k_{PAR} values) in the 0–20-m range. Hereinafter, we will refer to optical depth as “depth” for simplicity.

The main focus of this study is to introduce an ocean model with hybrid coordinates for the Black Sea, using the newly developed solar radiation penetration scheme. We then examine how solar radiation absorption alters the prediction of upper-ocean quantities. Hybrid Coordinate Ocean Model (HYCOM) is applicable to studies concerned with coastal and interior locations of the Black Sea because it behaves like a σ -coordinate model in shallow, unstratified coastal regions, like a z -level coordinate model in the mixed layer and other unstratified regions, and like an isopycnic-coordinate model where the open ocean is stratified. The model makes a dynamically smooth transition between the coordinate types via the layered continuity equation. The choice of coordinate type varies in time and space, and the optimal choice is updated every time step. In this paper, the effects of subsurface heating and atmospheric forcing on circulation dynamics of the Black Sea are examined, including its coastal and shelf regions and the interactions of these regions with the interior of the basin.

This paper is organized as follows: In section 2, spatial and temporal characteristics of attenuation depths from the remotely sensed data in the Black Sea are introduced, as well as a new formulation representing attenuation of solar radiation with depth. In section 3, basic features of HYCOM are given. In section 4, the set up of the Black Sea model is explained along with the atmospheric forcing used in the model. In section 5, the effects of ocean turbidity on the annual mean of the model simulations are discussed using atmospheric forcing from two different sources. The summary and conclusions are presented in section 6.

2. Solar radiation penetration

Penetration of solar radiation into the ocean has a strong spectral dependence with red and near-infrared (IR) radiation absorbed within ≈ 1 m of the surface and shorter wavelengths absorbed at greater depths (e.g., Lalli and Parsons 1997). The incident solar irradiance that penetrates to depths greater than 1 m is predominantly in the visible and ultraviolet (UV) bands, and this is regulated through absorption by the water, phytoplankton, and suspended particles. This latter portion of the spectrum is referred to as photosynthetically active radiation (PAR) because it is the light available for photosynthesis by phytoplankton (e.g., Liu et al. 1994). PAR accounts for 43%–50% of the solar irradiance at the sea surface (e.g., Rochford et al. 2001). The vertical

PAR distribution is a direct response to the intensity of incident solar irradiance flux entering at the sea surface (e.g., Austin and Petzold 1986) and its attenuation with depth (k_{PAR}).

As the light passes through water, it is both scattered and absorbed with different wavelengths of the visible spectrum penetrating to different depths. The influence of solar radiation differs depending on water type (Simonot and Le Treut 1986) because the attenuation depth in the ocean is quite variable over the global ocean (e.g., Kara et al. 2004). While fully spectral representations are available (Morel and Antonie 1994; Morel and Maritorena 2001), most ocean models use simple solar irradiance approximations based on a single exponential (e.g., Paulson and Simpson 1977; Schneider and Zhu 1998; Murtugudde et al. 2002; Kara et al. 2003). The reason is that, for water depths greater than 10 m, the penetrative solar flux can be accurately represented by a single exponential. Thus, OGCM studies only considered solar radiation that penetrates below the top layer or level of the model. In these cases, the red and near-infrared radiation is completely absorbed within the surface layer (e.g., minimum MLD of 10 m).

a. A new subsurface heating parameterization for OGCMs

An OGCM with high vertical resolution needs at least two bands of solar radiation penetration for the top 10 m of the water column. Traditional two-band Jerlov schemes differ significantly from single-band k_{PAR} between about 3 and 15 m, with k_{PAR} less absorptive than Jerlov near the surface (Fig. 2). This difference is primarily due to the Jerlov split between “red” (near surface) and “blue” (deep) light, with k_{PAR} assuming that the 51% nonvisible (primarily IR) light is absorbed at the surface and treats the remaining 49% (i.e., PAR) as one band that is biased toward blue. On the contrary, classical Jerlov types include both visible and IR light in its near surface red band and therefore has much less blue light, with the amount of blue light dependent on the turbidity. For example, the percentage of light remaining at about 2-m depth for Jerlov I, IA, IB, II, and III water types is 42%, 38%, 33%, 23%, and 22% (all primarily in the blue spectrum), respectively (Table 1).

Jerlov water types at 2 m are used to modify the single exponential formulation, $Q_{\text{sol}}(z)/Q_{\text{sol}}(0) = 0.49 \exp(-z k_{\text{PAR}})$, where $Q_{\text{sol}}(0)$ is the total shortwave radiation at the sea surface. Penetration depth scales are assumed for $k_{\text{PAR}} = 1/23, 1/20, 1/17,$ and $1/14$ because these are the blue extinction coefficients from existing schemes (Kara et al. 2005b). The fit is determined by finding a ratio, $\gamma = Q_{\text{blue}}(0)/Q_{\text{sol}}(0)$, such that

$$Q_{\text{sol}}(2)/Q_{\text{sol}}(0) = (1 - \gamma) \exp(-2/0.5) + \gamma \exp(-2k_{\text{PAR}}) \quad (1)$$

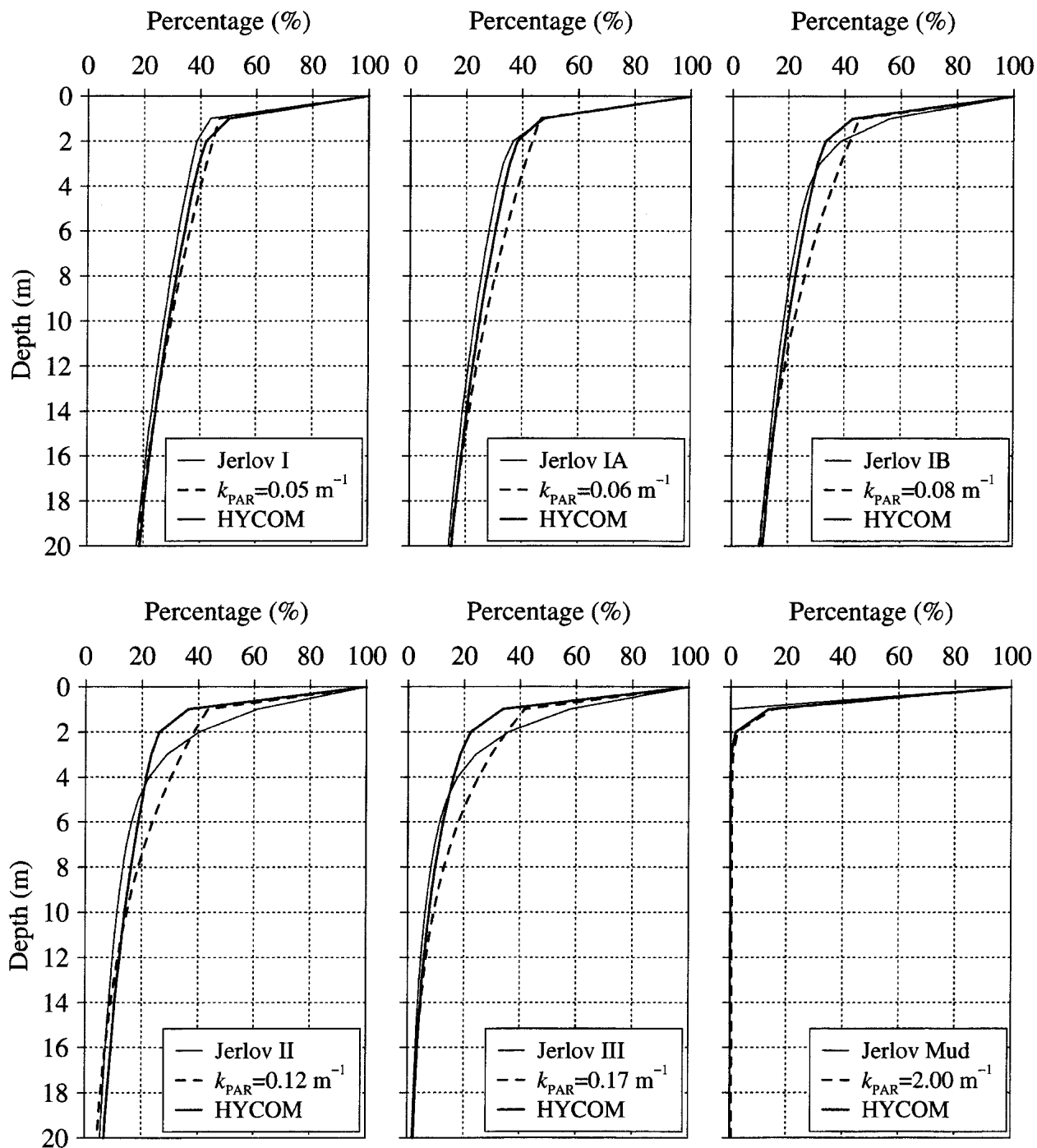


FIG. 2. Percentage of shortwave radiation remaining below the sea surface as a function of depth. The k_{PAR} values used in HYCOM are compared with those obtained from the traditional Jerlov approach (Jerlov I, IA, IB, II, III, and mud) and those used in a coarse-vertical-resolution OGCM, NLOM ($k_{PAR} = 0.05, 0.06, 0.08, 0.12, 0.17 \text{ m}^{-1}$, and mud). The HYCOM k_{PAR} values of 0.043 45, 0.0500, 0.0588, 0.0714, 0.1266, and 2.00 m^{-1} correspond to Jerlov I, IA, IB, II, III, and mud cases, respectively. HYCOM and NLOM use the spatially and temporally varying k_{PAR} climatology as processed from the daily averaged k_{490} dataset from SeaWiFS. Note that HYCOM uses a 0.5 m e -folding depth for the red spectrum, and so, as k_{PAR} approaches 2.0 m^{-1} , this indicates complete (or almost complete) absorption of the solar radiation within the mixed layer.

TABLE 1. Percentage of shortwave radiation remaining under the Jerlov extinction. The percentage values are given for each Jerlov class. Note this percentage incorrectly increases with increasing turbidity at 1- and 2-m depth.

Depth (m)	Jerlov I	Jerlov IA	Jerlov IB	Jerlov II	Jerlov III
0	100.00	100.00	100.00	100.00	100.00
1	43.54	47.86	55.76	60.95	57.57
2	38.69	36.60	38.40	40.24	35.77
3	36.87	33.12	31.00	28.98	24.20
4	35.30	31.19	27.31	22.63	17.74
5	33.79	29.61	25.04	18.84	13.88
6	32.36	28.15	23.35	16.39	11.37
7	30.98	26.78	21.92	14.67	9.60
8	29.66	25.47	20.64	13.36	8.25
9	28.40	24.23	19.44	12.28	7.17
10	27.19	23.05	18.33	11.26	6.20
11	26.03	21.92	17.28	10.48	5.47
12	24.93	20.85	16.29	9.76	4.82
13	23.87	19.84	15.36	9.09	4.24
14	22.85	18.87	14.48	8.46	3.74
15	21.88	17.95	13.66	7.88	3.29
20	17.60	13.98	10.18	5.51	1.75
30	11.40	8.48	5.65	2.70	0.49
40	7.38	5.14	3.14	1.32	0.14
50	4.78	3.12	1.74	0.65	0.04
60	3.09	1.89	0.97	0.32	0.01
70	2.00	1.15	0.54	0.15	0.00
80	1.30	0.70	0.30	0.08	0.00
90	0.84	0.42	0.17	0.04	0.00
100	0.54	0.26	0.09	0.02	0.00

matches the Jerlov table. The red spectrum penetration scale is 2 m (e -folding depth of 0.5 m) so that $\approx 98\%$ of this radiation component is absorbed within 2 m of the surface, which is represented by $\exp(-2/0.5)$. It should be noted that $\exp(-2/0.5)$ is 0.0183 (1.83%). This contribution to the ratio is large enough that it must be allowed for in the fit. Assuming that water types of I, IA, and IB are more important than the type II, the ratio is expressed as $\gamma = \max(0.27, 0.695 - 5.7k_{PAR})$ as shown in Fig. 3.

Thus, solar subsurface heating parameterizations are as follows:

$$Q_{sol}(z)/Q_{sol}(0) = (1 - \gamma) \exp(-z/0.5) + \gamma \exp(-z k_{PAR}), \quad (2)$$

$$\gamma = \max(0.27, 0.695 - 5.7k_{PAR}), \quad (3)$$

$$Q(z) = Q(0) + [Q_{sol}(0) - Q_{sol}(z)], \quad \text{and} \quad (4)$$

$$Q(0) = Q_{LW} + Q_L + Q_S, \quad (5)$$

where $Q(z)$ is net heat flux absorbed from the sea surface down to depth z , $Q(0)$ is net heat flux absorbed at the sea surface, Q_{LW} is the downward net longwave radiation, Q_L is the downward latent heat flux, and Q_S is the downward sensible heat flux. We adopted the convention that all heat flux terms are positive into the ocean. Note that HYCOM's "surface" heat flux is not $Q(0)$, but rather the near surface flux absorbed in layer 1 [e.g., $Q(3)$ when the top model layer is 3 m thick]. The

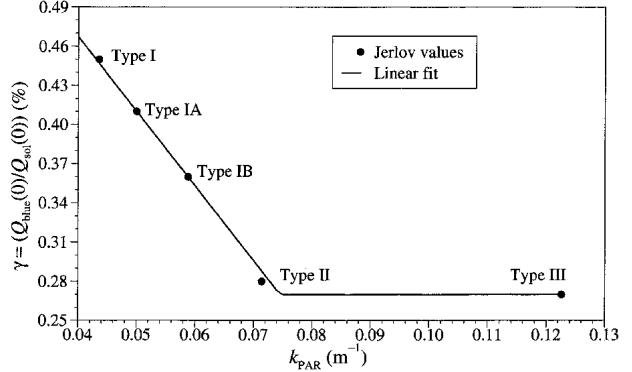


FIG. 3. Percentage changes of $\gamma = Q_{blue}(0)/Q_{sol}(0)$ with k_{PAR} . All PAR is assumed to represent primarily the blue spectrum. One band for the infrared (IR) and another for the PAR (a total of two bands) is adequate for approximating the subsurface heating with depth in basin- and regional-scale OGCMs, which is the primary interest when simulating upper-ocean features.

rate of heating/cooling of the each layer below layer 1 is simply obtained by evaluating $Q(z)$ or $Q_{sol}(z)$, at the bottom and top of the layer.

In the present shortwave radiation penetration parameterization (2), the red penetration scale is 2 m, and the blue penetration scale is $1/k_{PAR}$. The fraction of solar radiation (γ) in the blue band depends linearly on k_{PAR} for $k_{PAR} < 0.074 \text{ m}^{-1}$, and it is 0.27 for $k_{PAR} \geq 0.074 \text{ m}^{-1}$. The percentage of shortwave radiation under k_{PAR} extinction calculated using this approach is provided in Table 2. In Fig. 2 the new generalized k_{PAR} values are compared with the traditional Jerlov waters and the k_{PAR} approach based on a single band as used in Naval Research Laboratory (NRL) Layered Ocean Model (NLOM) with an embedded mixed layer (Wallcraft et al. 2003; Kara et al. 2003). It must be emphasized that in the NLOM subsurface heating parameterization 51% of $Q_{sol}(0)$ was nominally absorbed at the surface, because with a 10-m minimum surface layer thickness there was no need to resolve the penetration of red wavelengths. For HYCOM none of $Q_{sol}(0)$ is absorbed at the surface although $(1-\gamma)\%$ is absorbed very near the surface.

Although Lewis et al. (1990) and Siegel et al. (1995) indicated solar transmission at around 20-m depth can exceed 40 W m^{-2} for a surface irradiance of 200 W m^{-2} , this is possible only if $k_{PAR} \leq 0.04 \text{ m}^{-1}$ as evident from the results presented here, and if $k_{PAR} = 0.2 \text{ m}^{-1}$, 200 W m^{-2} becomes 1 W m^{-2} at 20 m (see Table 2). Earlier studies (e.g., Ohlmann et al. 1998) indicated that solar radiation in the visible band within the mixed layer below 10 m can be represented with a single exponential profile to within 10% accuracy. If 73% of the solar radiation is in the red exponential band, then as little as 4% of the total is left at 10 m based on present results.

The new parameterization presented here (i.e., k_{PAR} based on the Jerlov-like two-band scheme) is consistent with the one presented by Morel and Antonie (1994)

TABLE 2. Percentage of shortwave radiation remaining under the HYCOM k_{PAR} extinction based on $\gamma = Q_{\text{blue}}(0)/Q_{\text{sol}}(0)$ values. The percentage values are given for k_{PAR} values of 0.0400, 0.0435, 0.0500, 0.0588, 0.0714, 0.1266, 0.2000, 0.5000, and 2.0000 m^{-1} .

γ (%) Depth(m)	0.4670 0.0400	0.4472 0.0435	0.4100 0.0500	0.3597 0.0588	0.2879 0.0714	0.2700 0.1266	0.2700 0.2000	0.2700 0.5000	0.2700 2.0000
0	100.00	100.00	100.00	100.00	100.00	100.00	100.00	100.00	100.00
1	52.08	50.30	46.99	42.58	36.44	33.67	31.99	26.26	13.53
2	44.09	42.01	38.18	33.15	26.26	22.30	19.44	11.27	1.83
3	41.55	39.39	35.44	30.31	23.41	18.65	15.00	6.21	0.25
4	39.81	37.60	33.59	28.45	21.66	16.30	12.16	3.68	0.03
5	38.24	35.98	31.93	26.81	20.14	14.34	9.94	2.22	0.00
6	36.74	34.45	30.37	25.27	18.75	12.63	8.13	1.34	0.00
7	35.30	32.98	28.89	23.83	17.46	11.13	6.66	0.82	0.00
8	33.91	31.58	27.48	22.47	16.26	9.81	5.45	0.49	0.00
9	32.58	30.24	26.14	21.18	15.14	8.64	4.46	0.30	0.00
10	31.30	28.95	24.87	19.97	14.09	7.61	3.65	0.18	0.00
11	30.08	27.72	23.65	18.83	13.12	6.71	2.99	0.11	0.00
12	28.90	26.54	22.50	17.76	12.22	5.91	2.45	0.07	0.00
13	27.76	25.41	21.40	16.74	11.37	5.21	2.01	0.04	0.00
14	26.68	24.33	20.36	15.79	10.59	4.59	1.64	0.02	0.00
15	25.63	23.29	19.37	14.88	9.86	4.04	1.34	0.01	0.00
20	20.98	18.74	15.08	11.09	6.90	2.15	0.49	0.00	0.00
30	14.07	12.13	9.15	6.16	3.38	0.61	0.07	0.00	0.00
40	9.43	7.86	5.55	3.42	1.65	0.17	0.01	0.00	0.00
50	6.32	5.09	3.37	1.90	0.81	0.05	0.00	0.00	0.00
60	4.24	3.29	2.04	1.05	0.40	0.01	0.00	0.00	0.00
70	2.84	2.13	1.24	0.59	0.19	0.00	0.00	0.00	0.00
80	1.90	1.38	0.75	0.33	0.09	0.00	0.00	0.00	0.00
90	1.28	0.89	0.46	0.18	0.05	0.00	0.00	0.00	0.00
100	0.86	0.58	0.28	0.10	0.02	0.00	0.00	0.00	0.00

but computationally less expensive for global applications. Morel and Antonie (1994) use a three-band scheme (IR, red, and blue) with PAR that includes both red and blue bands, while the red band in the present parameterization consists of IR and red bands (i.e., nonPAR plus part of PAR).

The use of two optical bands, as introduced in this paper, is sufficient for ocean modeling studies unless an OGCM is coupled with a biological model that desires a full spectrum. When simulating the bio-optical properties of the ocean, the full spectral irradiance must be considered because of the sensitivity of the biology to selected wavelengths. For example, there is strong pigment absorption at 490 nm by phytoplankton and the variation in solar irradiance at this wavelength will control the rate of photosynthesis. Ignoring the spectral character of the PAR can result in underestimates of primary production by more than a factor of 2 (e.g., Laws et al. 1990; Morel and Maritorena 2001).

b. Attenuation depths in the Black Sea

Here, the interest is in the amount of shortwave radiation that penetrates through the mixed layer. Thus, spatial variations in the annual mean shortwave radiation over the sea surface are shown first (Figs. 4a,b). These fields were obtained from two sources: 1) the European Centre for Medium-Range Weather Forecasts (ECMWF) reanalysis (ERA-15) product (Gibson et al. 1999), and 2) the Fleet Numerical Meteorology and Oceanography Center (FNMOC) Navy Opera-

tional Global Atmospheric Prediction System (NOGAPS) data (Rosmond et al. 2002). An annual mean was formed over 1979–93 for ECMWF and 1998–2002 for NOGAPS. Later, we will use ECMWF and NOGAPS output to investigate model sensitivity to the choice of atmospheric forcing product. While the spatial distributions of shortwave radiation from ECMWF and NOGAPS are different, both generally have large values in the interior compared to coastal regions. The basin-averaged annual mean shortwave radiation values are 141 and 174 W m^{-2} for ECMWF and NOGAPS, respectively. The amount of shortwave radiation that enters the mixed layer depends on the attenuation depths as mentioned in section 2a.

The OGCM used (see section 3) takes solar radiation penetration into account through climatological monthly mean attenuations depths so that the subsurface heating can be prescribed in the model. For this purpose the monthly mean attenuation depths were obtained using a remotely sensed k_{490} dataset (McClain et al. 1998) acquired from the Sea-Viewing Wide Field-of-View Sensor (SeaWiFS) Project for the years 1997–2001. SeaWiFS ocean color data provide information on radiances emitted from the sea surface at selected wavelengths. From this information the wavelength dependence of the diffuse attenuation coefficient can be constructed using the PAR portion of the solar spectrum. The SeaWiFS monthly mean k_{490} datasets have a horizontal resolution of 9 km ($\approx 1/12^\circ$). Using these monthly k_{490} datasets, the monthly k_{PAR} climatologies

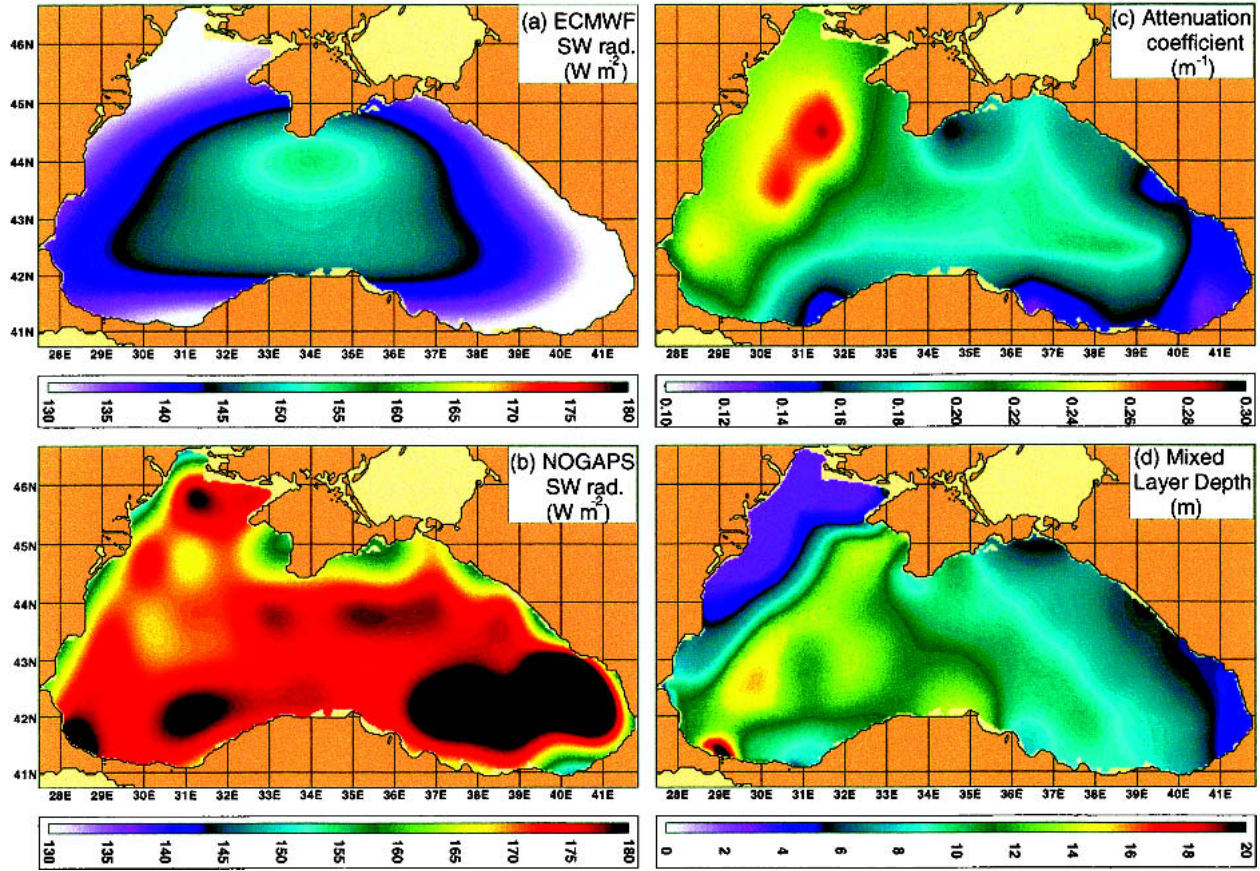


FIG. 4. Climatological annual mean of various quantities over the Black Sea: (a) incoming shortwave radiation at the sea surface ($W m^{-2}$) constructed from the $1.125^{\circ} \times 1.125^{\circ}$ ECMWF ERA product (1979–93); (b) shortwave radiation at the sea surface ($W m^{-2}$) constructed from the $1^{\circ} \times 1^{\circ}$ NOGAPS product (1998–2002); (c) attenuation coefficient of PAR (m^{-1}) processed from the $1/12^{\circ}$ SeaWiFS k_{490} data (1997–2001) as explained in the text, in detail; and (d) ocean MLD (m) based on the layer definition of Kara et al. (2000). The color bars for (a) and (b) are the same. Overall, differences between ECMWF and NOGAPS are mostly due to the time intervals over which the climatologies were constructed, 1979–93 for ECMWF and 1998–2002 for NOGAPS. Because the latter does not provide any thermal forcing prior to 1998, we had to form the climatology based on only 5 yr of model output. A comparison of the two (not shown) over the same time period (1998–2002) gave better agreement. The MLD is defined as the depth at the base of an isopycnal layer, where the density has changed by a varying amount of $\Delta\sigma_t = \sigma_t(T + \Delta T, S, P) - \sigma_t(T, S, P)$ from the density at a reference depth of 1 m based on a chosen ΔT (here $0.5^{\circ}C$). In this representation of MLD, S is the salinity, T is the temperature, and P is pressure set to zero.

were constructed using the Zaneveld et al. (1993) regression relations. Even though many scenes are used to construct the monthly means, the k_{490} data still have data voids due to cloud cover and infrequent sampling by satellite sensors, as well as incorrect and biased observations (noise). Thus, a statistical interpolation method (Daley 1991) was applied to fill in data voids. The monthly mean k_{PAR} fields were then computed from the k_{490} data and spatially interpolated to the HYCOM domain. These climatological monthly mean k_{PAR} fields, constructed over 1 October 1997–31 December 2001, were used for prescribing the subsurface heating in two of the HYCOM simulations discussed later.

For simplicity, the annual mean of the k_{PAR} processed from the SeaWiFS data is shown in Fig. 4c. The large k_{PAR} values are a typical feature of the attenua-

tion coefficient in the Black Sea. The decreased transparency over the most of the Black Sea is due to the greater biological productivity that occurs from increased availability of nutrients trapped in the euphotic zone by the shallow mixed layer with a sharp pycnocline at the base (e.g., Kideys et al. 2000; Konovalov and Murray 2001). For the present application, the greatest interest is in those situations where subsurface heating can occur below the mixed layer. Small attenuation depth ($1/k_{PAR}$) might produce complete (or almost complete) absorption of the solar radiation at the sea surface. In the western part, k_{PAR} values are usually greater than $0.25 m^{-1}$, which corresponds to an attenuation depth of 4 m. This attenuation depth implies that a turbidity increase in the region causes increased heating within the mixed layer because the climatological MLD is relatively shallow (Fig. 4d). The MLD was cal-

culated from monthly mean temperature and salinity profiles obtained from the new 1/4° Generalized Digital Environmental Model (GDEM) climatology (NAVOCEANO 2003) that includes 78 levels in the vertical direction. A variable density (σ_t) criterion with $\Delta T = 0.5^\circ\text{C}$ is used to obtain MLD. The reader is referred to Kara et al. (2000) for a more detailed definition of MLD.

3. HYCOM description

The model is a generalized [hybrid isopycnal/terrain-following (σ)/ z -level] coordinate primitive equation model whose original features are described in Bleck (2002). The hybrid coordinate extends the geographic range of applicability of traditional isopycnic coordinate circulation models toward shallow coastal seas and unstratified parts of the ocean. The vertical coordinate evaluation for HYCOM is discussed in Chassignet et al. (2003), and the mixed layer/vertical mixing options in HYCOM are evaluated in Halliwell (2004).

The original hybrid coordinate approach was accomplished using a hybrid vertical coordinate grid generator (Bleck 2002). Any remapper of this kind must be based on a full vertical profile that is consistent with the model fields (which represent vertical averages across each layer). The original remapper in HYCOM assumed that each field was constant in the vertical within each layer. This is the simplest possible profile, and it may be the best choice when remapping layers that are nearly isopycnal. However, when remapping layers that are far from isopycnal, this approach can lead to excessive diffusion. HYCOM's current remapper, as used in the Black Sea simulations presented in this paper, allows the profile to vary linearly across a layer if the layer is not close to being isopycnal, which significantly reduces diffusion. The remapping process can be thought of as finite-volume vertical advection (Leveque 2002); in these terms, the original remapper was using donor-cell upwind advection, and the latest remapper is using the piecewise linear method with a monotonized central-difference limiter (van Leer 1977).

The model contains a total of five prognostic equations: two momentum equations for the horizontal velocity components, a mass continuity or layer thickness tendency equation and two conservation equations for a pair of thermodynamic variables, such as salt and temperature or salt and density. The model equations, written in (x, y, s) coordinates, where s is an unspecified vertical coordinate, are

$$\frac{\partial \mathbf{v}}{\partial t_s} + \nabla_s \cdot \frac{\mathbf{v}^2}{2} + (\zeta + f)\mathbf{k} \times \mathbf{v} + \left(\frac{\partial s}{\partial t} \frac{\partial p}{\partial s} \right) \frac{\partial \mathbf{v}}{\partial p} + \nabla_s M - p \nabla_s \alpha = -g \frac{\partial \tau}{\partial p} + \left(\frac{\partial p}{\partial s} \right)^{-1} \nabla_s \cdot \left(\nu \frac{\partial p}{\partial s} \nabla_s \mathbf{v} \right), \quad (6)$$

$$\frac{\partial}{\partial t_s} \left(\frac{\partial p}{\partial s} \right) + \nabla_s \cdot \left(\mathbf{v} \frac{\partial p}{\partial s} \right) + \frac{\partial}{\partial s} \left(\frac{\partial s}{\partial t} \frac{\partial p}{\partial s} \right) = 0, \quad \text{and} \quad (7)$$

$$\frac{\partial}{\partial t_s} \left(\frac{\partial p}{\partial s} \theta \right) + \nabla_s \cdot \left(\mathbf{v} \frac{\partial p}{\partial s} \theta \right) + \frac{\partial}{\partial s} \left(\frac{\partial s}{\partial t} \frac{\partial p}{\partial s} \theta \right) = \nabla_s \cdot \left(\nu \frac{\partial p}{\partial s} \nabla_s \theta \right) + \hat{h}_\theta, \quad (8)$$

where $\mathbf{v} = (u, v)$ is the horizontal velocity vector, p is pressure, θ represents any one of the model's thermodynamic variables, $\alpha = 1/\rho$ is the potential specific volume, $\zeta = \partial v/\partial x_s - \partial u/\partial y_s$ is the relative vorticity, $M = gz + p\alpha$ is the Montgomery potential, $gz = \phi$ is the geopotential, f is the Coriolis parameter, \mathbf{k} is the vertical unit vector, ν is a variable eddy viscosity/diffusivity coefficient, and τ is the wind- and/or bottom-drag induced shear stress vector. The variable \hat{h}_θ represents the sum of diabatic source terms, including diapycnal mixing acting on θ . Subscripts show which variable is held constant during partial differentiation. Distances in x , y direction, as well as their time derivatives u and v , respectively, are measured in the projection onto a horizontal plane.

The prognostic equations in the model are time-integrated using a split-explicit treatment of barotropic and baroclinic modes (Bleck and Smith 1990). The split-explicit approach has proven to be advantageous for executing ocean models on massively parallel computers because it does not require solution of an elliptic equation. Isopycnal diffusivity and viscosity values, including the one used for thickness diffusion (interface smoothing), are formulated as $u_d \Delta x$, where Δx is the local horizontal mesh size and u_d is of order 0.01 m s^{-1} . In regions of large shear, isopycnic viscosity is set proportional to the product of mesh-size squared and total deformation (Smagorinsky 1963), the proportionality factor being 0.2.

HYCOM uses the K -profile parameterization (KPP) mixed layer model (Large et al. 1994), which is particularly attractive for several reasons. It contains improved parameterizations of physical processes in the mixed layer, including nonlocal effects. It has also been designed to run with relatively low vertical resolution, an advantage for OGCMs. The KPP model calculates the mixing profile from the surface to the bottom of the water column, and thus provides an estimate of diapycnal mixing beneath the mixed layer. It provides mixing throughout the water column with an abrupt but smooth transition between the vigorous mixing within the surface boundary layer and the relatively weak diapycnal mixing in the ocean interior. The KPP scheme has primarily been tuned against large-eddy simulations (LES) and therefore typically over short time scales (e.g., the diurnal cycle) and in small regions. In this paper, the main interest is in longer time scales (monthly) over the Black Sea.

The main quantities used throughout this paper are sea surface height (SSH) and MLD. The SSH is a diagnostic quantity, which is sum of the Montgomery potential and barotropic pressure (Kara et al. 2005a). The

MLD is a diagnostic quantity that depends on a specified density difference with respect to the surface. In general, the MLD is the shallowest depth at which the density change with respect to the surface is the equivalent of 0.2°C . Salinity-driven mixed layers can be accommodated by converting to density. The conversion is done at the surface (i.e., with respect to sea surface temperature and sea surface salinity), and so HYCOM converts the temperature change to a local density change and then finds the shallowest depth. The KPP mixed layer model is applied to every horizontal point independently. This procedure might sometimes lead to a very spatially noisy MLD. Thus, a uniform nine-point smoothing of the MLD fields is used throughout the analysis in this paper.

4. Black Sea model

a. Model resolution and constants

The Black Sea model used here has [$1/25^{\circ} \times 1/25^{\circ} \cos(\text{lat})$, longitude \times latitude] resolution on a Mercator grid. Zonal and meridional array sizes in the model are 360 and 206, respectively. The Mercator grid has square grid cells with a resolution of [$0.04 \cos(\text{lat}) \times 111.2 \text{ km}$]—that is, 3.37 km at the southern and 3.05 km at the northern coast. Average grid resolution is $\approx 3.2 \text{ km}$.

The model has 15 hybrid layers (10 predominantly isopycnal and 5 always z levels). The target density values (in σ_t) corresponding to layers 1–15 are 6.00, 9.00, 10.00, 11.00, 12.00, 12.80, 13.55, 14.30, 15.05, 16.20, 16.80, 16.95, 17.05, 17.15, and 17.20, respectively. Here, a detailed explanation is provided about how the vertical layers are distributed in the Black Sea model. One advantage of HYCOM is the generalized vertical coordinate. Typically, the model has isopycnal coordinates in the stratified ocean but uses the layered continuity equation to make a dynamically smooth transition to z levels (fixed-depth coordinates) in the unstratified surface mixed layer and σ levels (terrain-following coordinates) in shallow water. The optimal coordinate is chosen every time step using a hybrid coordinate generator. Thus, HYCOM automatically generates the lighter isopycnal layers needed for the pycnocline during summer. These become z levels during winter. The density values for the isopycnals and the decreasing change in density between isopycnal coordinate surfaces is based on the density climatology (see section 4c). The density difference values were chosen so that the layers tend to become thicker with increasing depth, with the lowermost abyssal layer being the thickest.

In general, HYCOM needs fewer vertical coordinate surfaces than, say, a conventional z -level model, because isopycnals are more efficient in representing the stratified ocean. For example, fewer isopycnals than z -levels are needed to resolve the pycnocline because 1) the isopycnals are Lagrangian coordinates that follow

the simulated depth of the chosen isopycnals with computational precision, and 2) isopycnal coordinates avoid the artificially large diapycnal diffusion that occurs in z -level and σ -coordinate models. This allows isopycnal models to maintain a sharp pycnocline without the diffusion that plagues z -level and σ -coordinate models. In contrast, z -level models must resolve the pycnocline by having high vertical resolution at all depths where the pycnocline may occur. The high vertical resolution is also needed to allow lower vertical diffusion coefficients below the mixed layer and thereby decrease the pycnocline diffusion. More z levels than isopycnals are also needed to resolve the bottom topography, which is represented by the bottom layer thickness in isopycnal models. In the unstratified mixed layer HYCOM uses z levels (in deep water) and needs the same high vertical resolution as a z -level model. However, we were able to use 3 m as the top layer thickness rather than 10 m as typically used in previous z -level models of the Black Sea because fewer coordinate surfaces were needed below the mixed layer.

Constant parameters used in the Black Sea model are provided in Table 3. The sensitivity of the Black Sea model to the choice of KPP parameters was investigated by undertaking a tuning exercise to find an optimal set in providing a realistic sea surface temperature (SST) from realistic atmospheric forcing over as much of the Black Sea as possible. This tuning was done by comparing the monthly satellite-based SST climatology to monthly averages from the model, which is similar to a statistical tuning methodology, such as introduced in Wallcraft et al. (2003). Overall, the original KPP constants reported in Large et al. (1994) worked best in the Black Sea model. The new KPP constants (e.g., the KPP value for turbulent shear contribution to bulk Ri number and the KPP value for calculating shear instability) suggested in Large et al. (1997) and Smyth et al. (2002) did not cause any significant changes in the model simulations.

b. Bottom topography

Most previous Black Sea model studies used UNESCO bathymetric maps to represent bottom topography (e.g., Stanev and Staneva 2001; Stanev and Staneva 2000), and a few studies used the Earth Topography Five Minute Grid (ETOPO5) data (e.g., Staneva et al. 2001). While ETOPO5 (NOAA 1988) is usually adequate for deeper parts of the ocean, it is less reliable over continental shelves ($< 200 \text{ m}$ deep) because of mismatches in the chart isobaths used in constructing the dataset. The use of ETOPO5 poses a problem for the Black Sea because some regions have a wide continental shelf.

The bottom topography in the Black Sea model (Fig. 5) was constructed from the Digital Bathymetric Data Base-Variable resolution (DBDB-V) dataset developed by the Naval Oceanographic Office (NAVOCEANO). The DBDB-1.0 (available online at

TABLE 3. Constant parameter values used in the HYCOM Black Sea simulations based on a series of tuning experiments. In the ocean interior, the contribution of background internal wave breaking, shear instability mixing, and double diffusion (both salt fingering and diffusive instability) are parameterized in the KPP model. In the surface boundary layer, the influences of wind-driven mixing, surface buoyancy fluxes, and convective instability are parameterized. The KPP algorithm parameterizes the influence of nonlocal mixing of temperature and salinity, which permits the development of countergradient fluxes.

Value	Description of the constant used in the Black Sea model
0.1	Deformation-dependent Laplacian viscosity factor
5.0×10^{-3}	Diffusion velocity for Laplacian momentum dissipation (m s^{-1})
67.0×10^{-4}	Diffusion velocity for biharmonic momentum dissipation (m s^{-1})
0.05	Diffusion velocity for biharmonic thickness dissipation (m s^{-1})
5.0×10^{-2}	Diffusion velocity for Laplacian temperature salinity diffusion (m s^{-1})
2.0×10^{-3}	Coefficient of quadratic bottom friction
10.0	Thickness of the bottom boundary layer (m)
0.02	Minimum density jump across interfaces (kg m^{-3})
0.2	Equivalent temperature jump across the mixed layer ($^{\circ}\text{C}$)
30.0	Reference mixed layer thickness for SSS relaxation (m)
0.3	KPP critical bulk Richardson number (Ri)
0.7	KPP value for calculating shear instability
50.0×10^{-4}	KPP max viscosity and diffusivity due to shear instability ($\text{m}^2 \text{s}^{-1}$)
1.0×10^{-4}	KPP background/interval wave viscosity ($\text{m}^2 \text{s}^{-1}$)
1.0×10^{-5}	KPP background/interval wave diffusivity ($\text{m}^2 \text{s}^{-1}$)
1.0×10^{-3}	KPP salt fingering diffusivity factor ($\text{m}^2 \text{s}^{-1}$)
1.9	KPP salt fingering factor
98.96	KPP value for nonlocal flux term
10.0	KPP value for nonlocal flux adjustment term
1.8	KPP value for turbulent shear contribution to the bulk Ri number
5.0	KPP value for the turbulent velocity scale

http://www7320.nrlssc.navy.mil/DBDB2_WWW/) used in HYCOM has a resolution of 1' (1 min). After interpolation to the Black Sea model grid, the final topography was smoothed twice with a nine-point smoother to reduce topographic energy generation at small scales poorly resolved by the model grid. In general, the Black Sea has an almost flat abyssal plain, a flat wide shelf in the northwestern part, and a steep continental slope along the Turkish coast (see Fig. 5).

c. Temperature and salinity initialization

Previous modeling studies of the Black Sea were limited to the use of local datasets constructed from sparse observations for the initial temperature and salinity climatologies (e.g., Altman et al. 1987; Stanev 1990). There is also uncertainty in the quality of these existing data sources in the Black Sea (e.g., Staneva and Stanev 1998). A well-documented commonly used subsurface temperature and salinity climatology from the $1^{\circ} \times 1^{\circ}$ *World Ocean Atlas 1994* (Levitus et al. 1994; Levitus

and Boyer 1994) does not cover the Black Sea region. While a recently updated *World Ocean Atlas* (Conkright et al. 2002) includes monthly mean temperature and salinity climatologies, it is still at $1^{\circ} \times 1^{\circ}$ grid resolution, which does not resolve the coastal and shelf regions. Thus, the Black Sea suffers from a lack of quality, fine-resolution subsurface temperature and salinity climatologies that can be used for model initialization.

Here, HYCOM is initialized using the temperature and salinity from the Modular Ocean Data Assimilation System (MODAS) climatology developed at NRL (Fox et al. 2002) because it provides increased horizontal resolution. The climatology has variable grid resolution: $1/8^{\circ}$ near land, $1/4^{\circ}$ over shallow shelves, and $1/2^{\circ}$ in the open ocean. This makes the MODAS climatology a candidate to use in studying the surface circulation. In general, the MODAS climatology is one of the current U.S. Navy standard tools for production of three-dimensional grids of temperature and salinity, and derived quantities such as density (Harding et al. 1999). MODAS includes both a static climatology and a dynamic climatology. The former represents the historical averages and is used here. Climatological potential temperature, salinity and density fields from MODAS are output at 27 depth levels ranging from 0 to 2200 m for the Black Sea (Fig. 6). While previous studies (e.g., Murray et al. 1991; Ozsoy et al. 1993) described the Black Sea as a two-layer system with a thin low-salinity surface layer overlying a relatively uniform higher-salinity deep layer, a four-layer system based on the high-vertical-resolution data from MODAS is evident from Fig. 6. Salinity increases from 17.8 psu at the sea surface to 23.0 psu at 500 m. The Cold Intermediate Layer (CIL) is characterized by temperatures less than $\approx 8.5^{\circ}\text{C}$, which occurs within a typical depth range of about 40–130 m overlying the main pycnocline where vertical stratification is maintained by the salinity gradient.

d. Wind and thermal forcing

HYCOM reads in the following time-varying atmospheric forcing fields: wind stress and thermal forcing (air temperature and air mixing ratio at 10 m above the sea surface, net shortwave radiation and net longwave radiation at the sea surface). For the Black Sea model wind/thermal forcing was constructed from two different archived operational weather center products: 1) $1.125^{\circ} \times 1.125^{\circ}$ ECMWF ERA-15 climatology (1979–93), and 2) $1^{\circ} \times 1^{\circ}$ NOGAPS climatology (1998–2002).

All model simulations are performed using climatological monthly mean forcing fields. However, a high-frequency component is added to the climatological forcing because the mixed layer is sensitive to variations in surface forcings on time scales of a day or less (e.g., Wallcraft et al. 2003; Kara et al. 2003) and because the future goal is to perform simulations forced by high-frequency interannual atmospheric fields from operational weather centers. Hybrid winds consist of monthly ECMWF (or NOGAPS) plus ECMWF wind anomaly

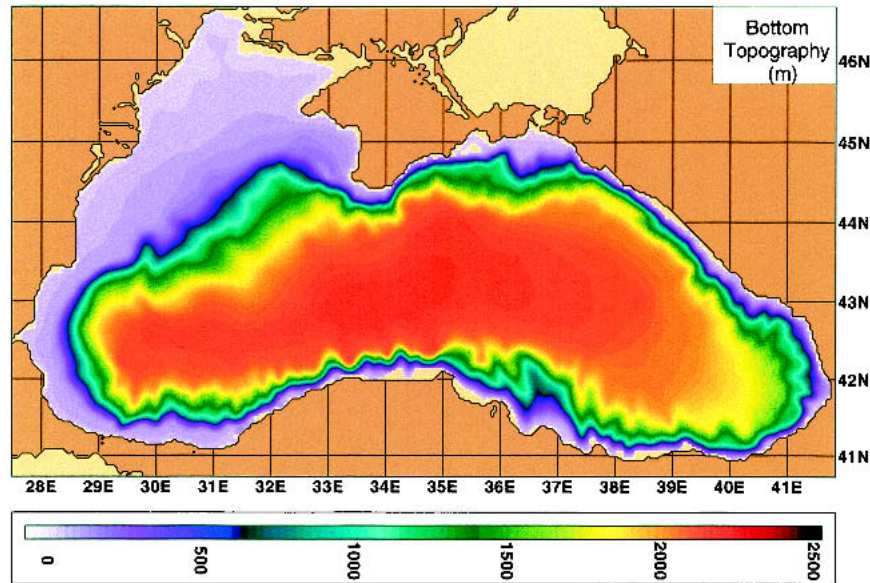


FIG. 5. The bottom topography (m) and the model coastline used in HYCOM simulations. The model land–sea boundary is the 10-m isobath. Water depths <10 m are light tan in color. The Sea of Azov is excluded in the model simulations. The abyssal plain of the Black Sea is ≈ 2000 m deep, and the maximum depth is ≈ 2204 m. The basin does not include large gulfs or islands but one of the most interesting features is the narrow continental shelf. Canyons are also evident in the bottom topography. The bottom topography includes 1-min DBDB-V data. The DBDB-V dataset was developed by the Naval Oceanographic (NAVOCEANO) to support the generation of bathymetric chart products. It provides bathymetric data to be integrated with other geophysical and environmental parameters for ocean modeling. The digitally rendered contours are put through a gridding routine. This routine takes the values that fall within a grid node area of influence, utilizing a multistage minimum-curvature spline algorithm.

lies. Construction of the ECMWF hybrid winds is briefly described here. The same procedure is applied to NOGAPS. For HYCOM wind stress forcing (τ_{HYCOM}), 6-h intramonthly anomalies from ECMWF are used in combination with the monthly mean wind stress climatology of ECMWF (NOGAPS) interpolated to 6-hourly intervals. The 6-h anomalies are obtained from a reference year. For that purpose, the winds from September 1994 through September 1995 (6 h) are used, inclusive, because they represent a typical annual cycle of the ECMWF winds, and because the September winds in 1994 and 1995 most closely matched each other. The 6-h September 1994 and September 1995 wind stresses are blended to make a complete annual cycle, which is denoted by τ_{ECMWF} . The ECMWF wind stresses are calculated from ECMWF 10-m winds using the bulk formulas of Kara et al. (2002). Monthly averages are first formed from the September 1994–September 1995 ECMWF wind stresses (τ_{ECMWF}) to create the ECMWF wind stress anomalies (τ_A), and are then linearly interpolated to the time intervals of the 6-h ECMWF winds to produce a wind stress product (τ_f). The anomalies are then obtained by applying the difference ($\tau_A = \tau_{\text{ECMWF}} - \tau_f$). Scalar wind speed is obtained from the input wind stress and therefore has 6-hourly variability. Note that NOGAPS provides sur-

face stress directly so the high frequency component (τ_A) is added to the interpolated monthly mean wind stress from NOGAPS.

The subsurface heating parameterizations used in HYCOM are already discussed in section 2a, in detail. The shortwave radiation at depth z [i.e., $Q_{\text{sol}}(z)$ in (2)] involves spatially and temporally varying monthly k_{PAR} climatology as processed from the daily averaged k_{490} dataset from SeaWiFS covering the Black Sea over 1 October 1997–31 December 2001. Thus, HYCOM reads in monthly mean k_{PAR} fields to include effects of water turbidity. The monthly mean turbidity variability over the Black Sea is examined in Kara et al. (2005a), in detail (see Fig. 4c for the annual mean). The Black Sea is very turbid with a basin-averaged climatological annual mean k_{PAR} value of 0.19 m^{-1} .

The net heat flux absorbed from the sea surface down to depth z is parameterized in (4), from which the rate of heating/cooling of each layer is obtained. Latent and sensible heat fluxes at the air–sea interface are calculated using efficient and computationally inexpensive bulk formulas that include the effects of dynamic stability (Kara et al. 2002). The combination of accuracy and ease of computation makes this method preferred for computing air–sea fluxes in HYCOM. Note that both sensible and latent heat fluxes are calculated using

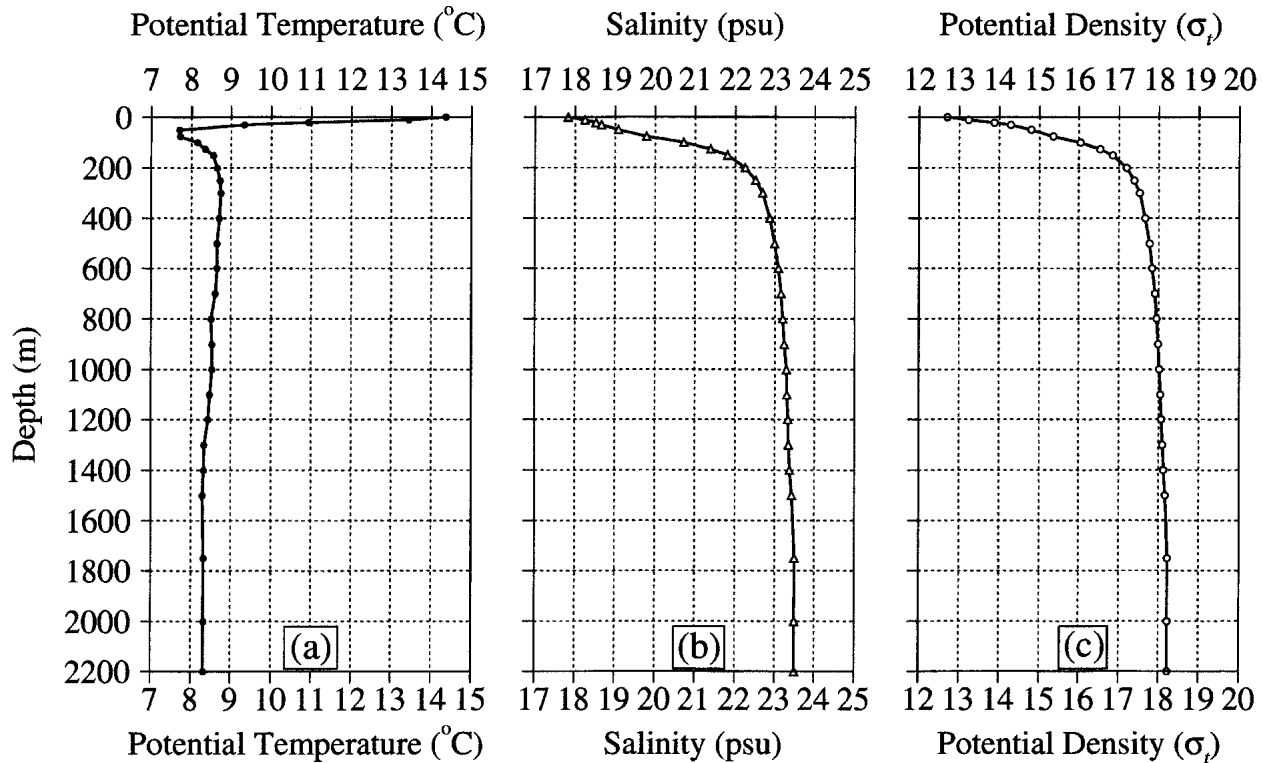


FIG. 6. Annual mean of basin-averaged potential temperature, salinity, and potential density profiles obtained from the MODAS climatology. Standard depth levels in the climatology are 0, 10, 20, 30, 50, 75, 100, 125, 150, 200, 250, 300, 400, 500, 600, 700, 800, 900, 1000, 1100, 1200, 1300, 1400, 1500, 1750, 2000, and 2200 m. The MODAS climatology does not include temperature/salinity below 1750 m in the Black Sea because the climatology is relaxed to the *World Ocean Atlas 1994* in deeper layers, which is void of data in this region. In this case, a simple linear extrapolation was applied to the temperature and salinity data, and then the profiles were extended down to ≈ 2200 m. This linear interpolation is reasonable given the fact that temperature and salinity of the deep water masses do not change very much on the climatological time scales and thus can be considered as quasi-steady.

model top layer temperature at each model time step. Including air temperature and model SST in the formulations for latent and sensible heat flux automatically provides a physically realistic tendency toward the correct SST. Radiation flux (net shortwave and net longwave fluxes) is so dependent on cloudiness that it is taken directly from ECMWF (or NOGAPS) for use in the model.

The Black Sea model treats rivers as a “runoff” addition to the surface precipitation field. The flow is first applied to a single ocean grid point and smoothed over surrounding ocean grid points, yielding a contribution to precipitation in meters per second. This works independently of any other surface salinity forcing. Looking more closely at the largest rivers in a given ocean model domain is important to represent evaporation and precipitation effects properly. However, the problem is knowing which data source is most accurate. There are several readily available river discharge climatologies, and climatological annual mean river flow values are constructed from these sources (Table 4) for each river discharged into the Black Sea (Table 5). HYCOM reads in monthly mean river discharge values. The

monthly mean RivDIS climatology (Vörösmarty et al. 1997, 1998) is preferred for use in HYCOM because it gives river inflow values at the mouth of the river. A total of six major rivers are used as precipitation forcing. The Danube River has the largest discharge with a river flow of $6365.0 \text{ m}^3 \text{ s}^{-1}$ (0.006365 Sv , where $1 \text{ Sv} \equiv 10^6 \text{ m}^3 \text{ s}^{-1}$). In the simulations described here HYCOM does not include the direct Bosphorus inflow, causing an imbalance in evaporation minus precipitation. This imbalance in the simulations was handled by adding a negative river precipitation (i.e., a river evaporation) for the Bosphorus.

e. Model simulations

Climatologically forced model simulations that use three different sets of k_{PAR} values are performed to investigate the effects of ocean turbidity on the sea surface circulation. Table 6 gives a brief explanation of each simulation. For experiment (expt) 1, spatially and monthly varying k_{PAR} values interpolated to the HYCOM grid are used. For expt 2, all solar radiation is absorbed at the sea surface by using an unrealistically large k_{PAR} value of 99.9 m^{-1} . For expt 3, the ocean

TABLE 4. Annual mean flow values obtained from four climatological datasets for the rivers discharged into the Black Sea. The source for the Perry data is Perry et al. (1996), RivDIS (see online at <http://daac.ornl.gov/rivdis/>), and UCAR (see online at <http://dss.ucar.edu/datasets/ds552.1/>). The final data product was constructed at NRL using the Perry dataset. The NRL dataset is similar to RivDIS except to a scale factor obtained from Perry et al. (1996) to correct the annual mean. The NRL database is designed to combine the best properties of the other databases into a single consistent global dataset with monthly mean river discharges and verified river mouth locations. The NRL dataset is consistent with RivDIS and Perry data as seen from the annual mean river discharge values. Thus the use of river discharge values from RivDIS or NRL is suitable in the Black Sea. The Perry dataset is a compilation of data from many sources and had one mean value for each river. Note that $1 \text{ Sv} \equiv 10^6 \text{ m}^3 \text{ s}^{-1} \approx 32\,000 \text{ km}^3 \text{ yr}^{-1}$. There are other rivers that are not listed in the table, such as the Southern Bug (Ukraine) and Kamtehiya (Bulgaria), which discharge into the Black Sea; however, they are not input to the model because the contributions from these rivers are very small. The Bosphorus is considered as a negative precipitation point to balance the evaporation minus precipitation field over the Black Sea.

River	Perry ($\text{m}^3 \text{ s}^{-1}$)	RivDIS ($\text{m}^3 \text{ s}^{-1}$)	UCAR ($\text{m}^3 \text{ s}^{-1}$)	NRL ($\text{m}^3 \text{ s}^{-1}$)
Danube	6365.0	6499.0	6413.6	6365.1
Dniepr	1630.8	1482.2	1483.7	1630.2
Rioni	409.7	408.6	402.7	409.7
Dniestr	326.3	375.2	324.3	326.3
Sakarya	217.3	192.3	192.8	217.4
Kizilirmak	180.5	201.8	202.2	202.2

River	Perry ($\text{km}^{-3} \text{ yr}^{-1}$)	RivDIS ($\text{km}^3 \text{ yr}^{-1}$)	UCAR ($\text{km}^3 \text{ yr}^{-1}$)	NRL ($\text{km}^3 \text{ yr}^{-1}$)
Danube	203.7	205.0	205.2	203.7
Dniepr	52.2	46.7	47.5	52.2
Rioni	13.1	12.9	12.9	13.1
Dniestr	10.4	11.8	10.4	10.4
Sakarya	7.0	6.1	6.2	7.0
Kizilirmak	5.8	6.4	6.5	6.5

turbidity over the Black Sea is set to a constant, $k_{\text{PAR}} = 0.06 \text{ m}^{-1}$, which is a representative value for clear water (e.g., Kara et al. 2004). Simulation experiments 1, 2, and 3 use wind/thermal forcing from ECMWF, while expts 4, 5, and 6 are essentially twins of expts 1, 2, and 3 but use wind/thermal forcing from NOGAPS. All of the HYCOM simulations presented in this paper were performed with no assimilation of any oceanic data except initialization from climatology and relaxation to sea

surface salinity. The model was run until it reached statistical equilibrium using 6-hourly climatological forcing as described earlier. It takes about 5–8 model years for a simulation to reach equilibrium.

5. Results and discussion

In this section, the sensitivity of model results to water turbidity is examined with a particular focus on upper ocean currents and sea surface height. All model results are presented based on annual means that were constructed from the last 4 yr of the model simulations. At least a 4-yr mean was needed because the 3.2-km HYCOM is nondeterministic and flow instabilities are a major contribution at this resolution.

The surface circulation in the Black Sea is dominated by meanders, eddies, and dipole structures (e.g., Oguz and Besiktepe 1999). This is evident from surface current and SSH snapshots from the 3.2-km HYCOM simulations (Fig. 7). Given that the Rossby radius of deformation in the Black Sea is $\approx 20\text{--}25 \text{ km}$, it is clear that the radii of coastal eddies in the model range from 1 to a few times the radius of deformation and are especially prevalent in the eastern half of the Black Sea. This result is somewhat consistent with the results reported from a $1/12^\circ$ ($\approx 9.0 \text{ km}$) z -level OGCM (Staneva et al. 2001), which was forced with monthly mean atmospheric variables (Sorkina 1974; Altman and Kumish 1986). When using different atmospheric forcing products, the location and number of eddies in the simulations are quite different in some regions, especially in the easternmost Black Sea (e.g., off Trabzon). In the case of ECMWF wind/thermal forcing (expt 1) there are almost no eddies present near the Sea of Azov; while, two small eddies exist in the case of NOGAPS wind/thermal forcing (expt 4). In addition to the differences in the sizes and locations of the small eddies, the SSH values for expts 1 and 4 are also different by up to $\approx 8 \text{ cm}$ in some regions, especially near the northeastern coast.

The HYCOM simulations do not exhibit significant changes in the surface circulation and SSH when all radiation is absorbed in the surface layer (expts 2 and 5) rather than using the solar radiation penetration scheme involving realistic attenuation depths (expts 1 and 4). This results from the high Black Sea turbidity.

TABLE 5. Time periods over which climatological river discharges were constructed. Total number of years for the climatology is also included. Note that the Perry dataset was constructed using the annual mean for individual years, and so the total number of years represents the total of these individual years. The other two datasets were constructed using monthly mean discharge values.

River	Perry		RivDIS		UCAR	
	Climatology	Years	Climatology	Years	Climatology	Years
Danube	1962–94	14	1921–84	64	1921–2000	80
Dniepr	1962–94	10	1952–84	33	1952–84	33
Rioni	1975–94	3	1965–84	20	1928–84	57
Dniestr	1975–91	4	1965–84	20	1881–1985	76
Sakarya	1975–91	3	1976–83	8	1976–83	8
Kizilirmak	1975–91	2	1976–83	8	1976–83	8

TABLE 6. Six HYCOM simulations presented in this study. The simulations were performed using several massively parallel supercomputers. The model array size is 360×206 for each layer, and performing a 1-month simulation takes ≈ 2.3 wall-clock hours using 64 IBM SP POWER3 processors or ≈ 0.7 wall-clock hours using 64 HP/COMPACT SC45 processors. A linear regression analysis was performed for domain averaged quantities (layer temperature, salinity, potential, and kinetic energy, etc.) to investigate statistical equilibrium in each layer, and is expressed numerically as percent change per decade. The model is deemed to be in statistical equilibrium when the rate of potential energy change is acceptably small (e.g., $<1\%$ in 5 yr) in all layers. The model uses climatological wind and thermal forcing (i.e., air temperature at 10 m, air mixing ratio at 10 m, shortwave and longwave radiation) constructed from ECMWF ERA-15 or NOGAPS products as explained in detail in the text.

Expt	k_{PAR}	Description of the experiment	Forcing
1	Variable	Spatial and temporal attenuation depths	ECMWF
2	99 m^{-1}	All solar radiation absorbed at the surface	ECMWF
3	0.06 m^{-1}	Clear water constant attenuation depth of 16.7 m	ECMWF
4	Variable	Spatial and temporal attenuation depths	NOGAPS
5	99 m^{-1}	All solar radiation absorbed at the surface	NOGAPS
6	0.06 m^{-1}	Clear water constant attenuation depth of 16.7 m	NOGAPS

In contrast, the clear water constant attenuation depth assumption (i.e., $k_{\text{PAR}} = 0.06 \text{ m}^{-1} \approx 17 \text{ m}$) in expts 3 and 6 shows quite different surface circulation structure and SSH variability, mostly east of 39°E where attenuation coefficients (depths) are small (large) in comparison with other parts of the region (see Fig. 4c). This result may seem unexpected. The reason is that even though the turbidity in the eastern Black Sea is relatively low in comparison with other regions of the Black Sea, it is still high in comparison with most of the global ocean (Kara et al. 2004). In addition, the seasonal cycle is relatively strong in the eastern Black Sea, and it has a strong mesoscale variability component associated with it (e.g., Stanev and Staneva 2000).

Based on the annual mean surface currents and SSH fields (Fig. 8), the clear water constant attenuation depth assumption (expts 3 and 6) results in different current structure in comparison to the standard cases (expts 1 and 4) in the eastern Black Sea. The SSH variability in the eastern gyre and off Sinop is also different (see Fig. 7). In general, as indicated in Ozsoy and Unluata (1997), the coastal eddies which have time scales of only a few days usually merge, causing the larger eddies to form on longer time scales as is evident in the HYCOM annual mean surface current fields. There is a permanent current system (the so-called Rim Current) encircling the Black Sea basin cyclonically over the continental slope. It is accompanied by a series of persistent anticyclonic mesoscale eddies as well as transient waves with mesoscale eddies propagating cyclonically around the basin.

The large-scale cyclonic circulation in the Black Sea is driven by the wind stress curl. This is a well-known feature of the Black Sea as previously noted in other OGCM studies (e.g., Stanev and Beckers 1999; Kourafalou and Stanev 2001). However, it is also clear that this feature is largely independent of the atmospheric forcing product choices made here. These results are not entirely consistent with previous OGCM studies. For example, Stanev and Beckers (1999) used a three-dimensional primitive equation GHER 3D model with a resolution of $15 \text{ km} \times 12 \text{ km}$. They reported the lowest SSH values in the eastern cyclonic gyre, indicating substantial differences in the wind stress, since this pattern is controlled by the wind stress curl. The 3.2-km HYCOM with a finer resolution than the GHER 3D also has realistic lowest values in the western cyclonic gyre for both ECMWF and NOGAPS forcing cases (expts 1 and 4, respectively).

Another important feature of the surface currents seen in all the HYCOM simulations is a well-defined mean eddy south of 43°N between 34° and 36°E (Fig. 8), which is known as the Sinop eddy, and which is missing from the annual mean surface current map of Stanev and Beckers (1999). In an analysis of hydrographic data by Oguz et al. (1993), the Sinop anticyclonic eddy emerged as one of dominant features of the Black Sea circulation, a result consistent with the HYCOM simulations.

A zonal temperature cross-sectional analysis is performed along 42.62°N (Fig. 9) to explain the differences in stratification seen in expts 1, 2, and 3 (also expts 4, 5, and 6). This section was chosen because it crosses major current systems including the mean eddy off Sinop (see Figs. 1 and 8). The main purpose is to examine how the subsurface heating affects annual mean stratification and surface circulation, which demonstrates dramatically the impact of turbidity on stratification, MLD and SST. Absorbing all radiation at the surface (expts 2 and 5) does yield a sharper thermocline but does not cause any major difference in comparison with the standard cases (expts 1 and 4). The stratification is obviously deeper and weaker when using a constant attenuation coefficient value of 0.06 m^{-1} (see Figs. 9c,f), as expected. This result is because of increased shortwave radiation below the sea surface. For example, $\approx 18\%$ is absorbed below 20 m (see Fig. 2). Thus, using the clear water constant attenuation depth, rather than realistic attenuation depths from SeaWiFS, results in excessive warming below the mixed layer. For example, the depth of the 11.5°C isotherm is $\approx 20 \text{ m}$ in expt 1, while it is $\approx 35 \text{ m}$ in expt 3.

In general, using a clear water constant attenuation depth assumption in the HYCOM simulations (expts 3 and 6) results in a relatively deep MLD in comparison with the standard simulations (expts 1 and 4), which used realistic attenuation depths (Fig. 10). The reason is that the warming of the water column below the mixed

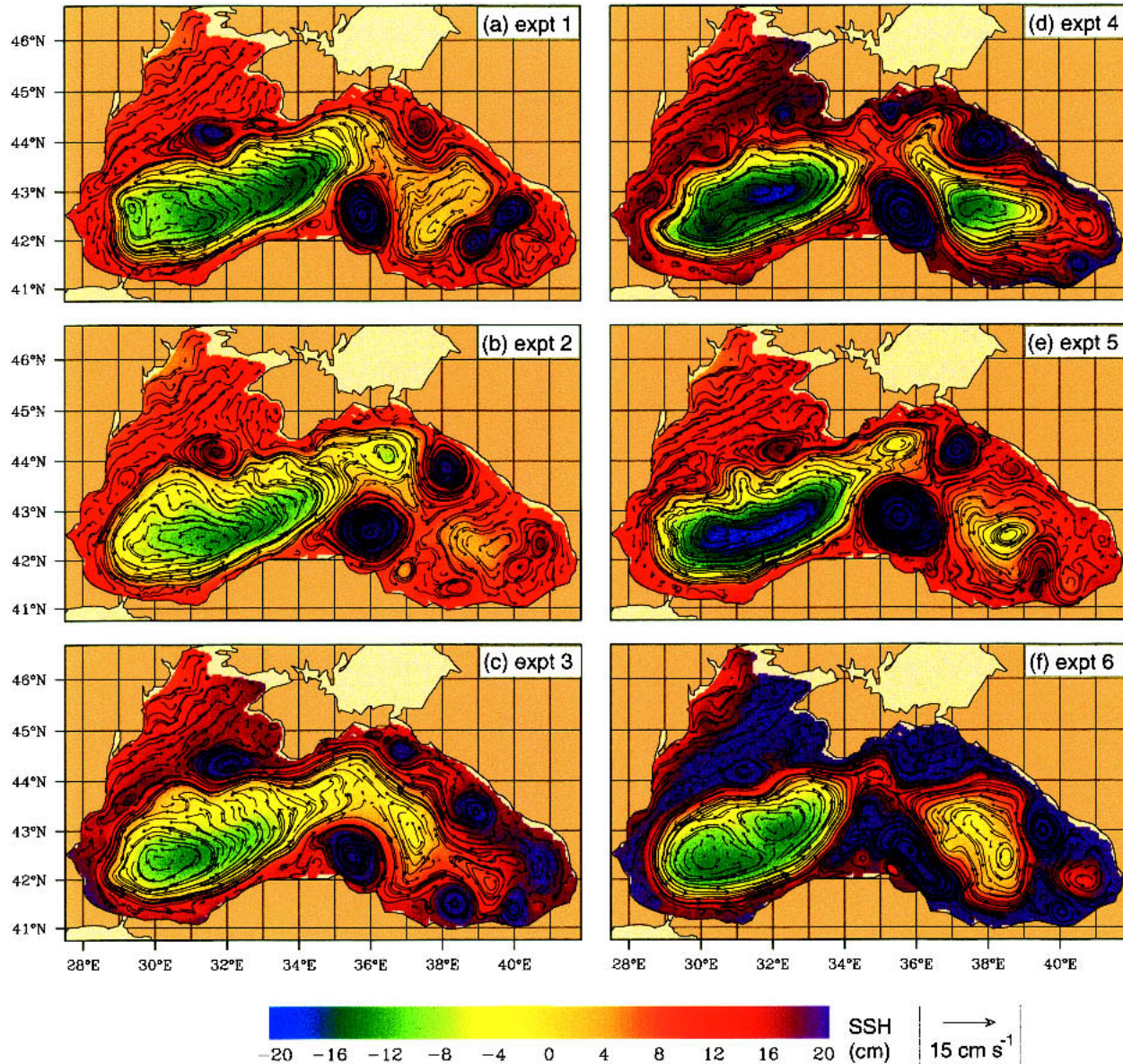


FIG. 7. Snapshots of sea surface currents (cm s^{-1}) displayed over sea surface height (cm) in the Black Sea on 2 Mar: (a) expt 1, (b) expt 2, and (c) expt 3 when HYCOM was forced with ECMWF wind and thermal fluxes; (d) expt 4, (e) expt 5, and (f) expt 6 when HYCOM was forced with NOGAPS wind and thermal fluxes. The length of the reference velocity vector is 15 cm s^{-1} . The velocity vectors are subsampled for plotting. See section 4d in the text for construction of the wind and thermal forcing fields.

layer leads to a weakening of the stratification, and this facilitates deepening of the mixed layer. This result is particularly evident in the deep MLD and less organized stratification between 34° and 37°E off Sinop, especially in expt 6.

In comparison with the climatological MLD (see Fig. 4d), the root-mean-square (rms) differences are ≈ 5.7 , 5.6 , and 10.1 m for expts 1, 2, and 3, respectively, using the methodology of Kara et al. (2000) to calculate the MLDs. This means that using a constant attenuation depth value of 17 m in expt 3 gave an rms difference increase in MLD of $\approx 77\%$ (i.e., from 5.7 to 10.1 m).

Similar rms differences were found for expts 4, 5, and 6 with values of 6.3 , 6.3 , and 10.9 m, respectively. Thus, using a clear water constant attenuation depth value yielded unrealistically deep MLDs for both atmospheric forcing sets. Associated with the strong stratification near the surface (Figs. 9a, d) and the variation in the MLD rms deviation from climatology are substantial changes in the subsurface temperatures and thermal stratification (Figs. 9c, f). Overall, subsurface temperatures from the standard simulations (expts 1 and 4) also agree better with those from the MODAS climatology than expts 3 and 6.

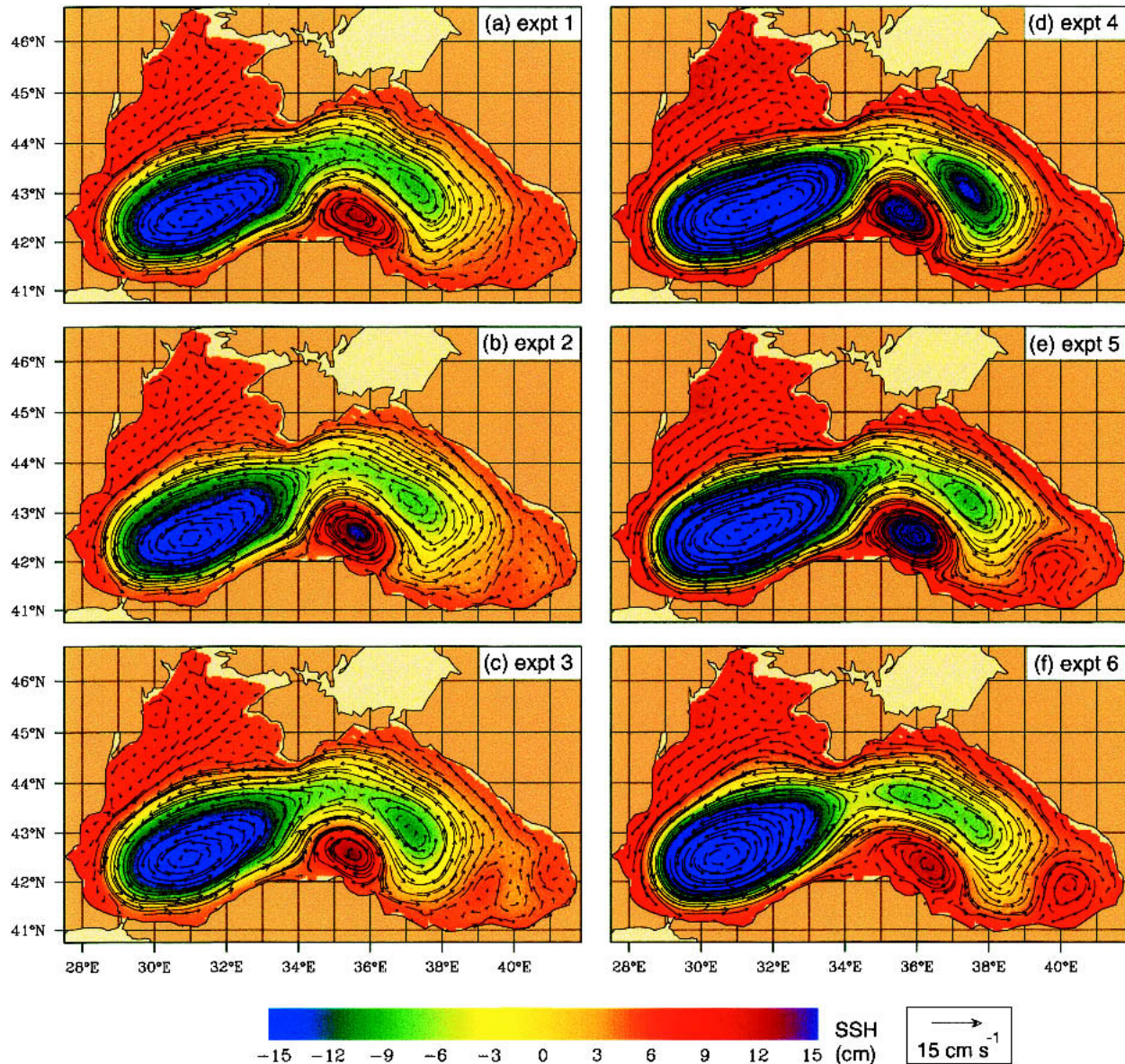


FIG. 8. As in Fig. 7, but for annual mean sea surface currents (cm s^{-1}) displayed over annual mean sea surface heights (cm) in the Black Sea. The annual mean was formed using model years 5–8. Each field has basinwide mean SSH anomaly of zero. The velocity vectors are subsampled for plotting.

Last, the synoptic space–time scales of optical property variability have not been considered in this paper. The reason is that a multiyear monthly average k_{PAR} climatology is used from SeaWiFS for turbidity. The actual turbidity will have short time scales (<1 month) and interannual variability. In addition this variability may be correlated with physical oceanic features, such as fronts and eddies, that are present in the ocean model but not well represented in the SeaWiFS climatology. The only ways to overcome this limitation would be to add an accurate biological model to the HYCOM simulations or to use synoptic turbidity ob-

servations and a data assimilative ocean model (assimilating satellite altimeter and other data). Both of these measures are outside the scope of this paper. Given the magnitude of the clear water versus the “actual” turbidity signal, the fundamental results of this paper should not be changed by a more accurate best-turbidity simulation.

6. Summary and conclusions

The purpose of this research is to 1) develop a solar radiation penetration scheme for OGCMs that uses at-

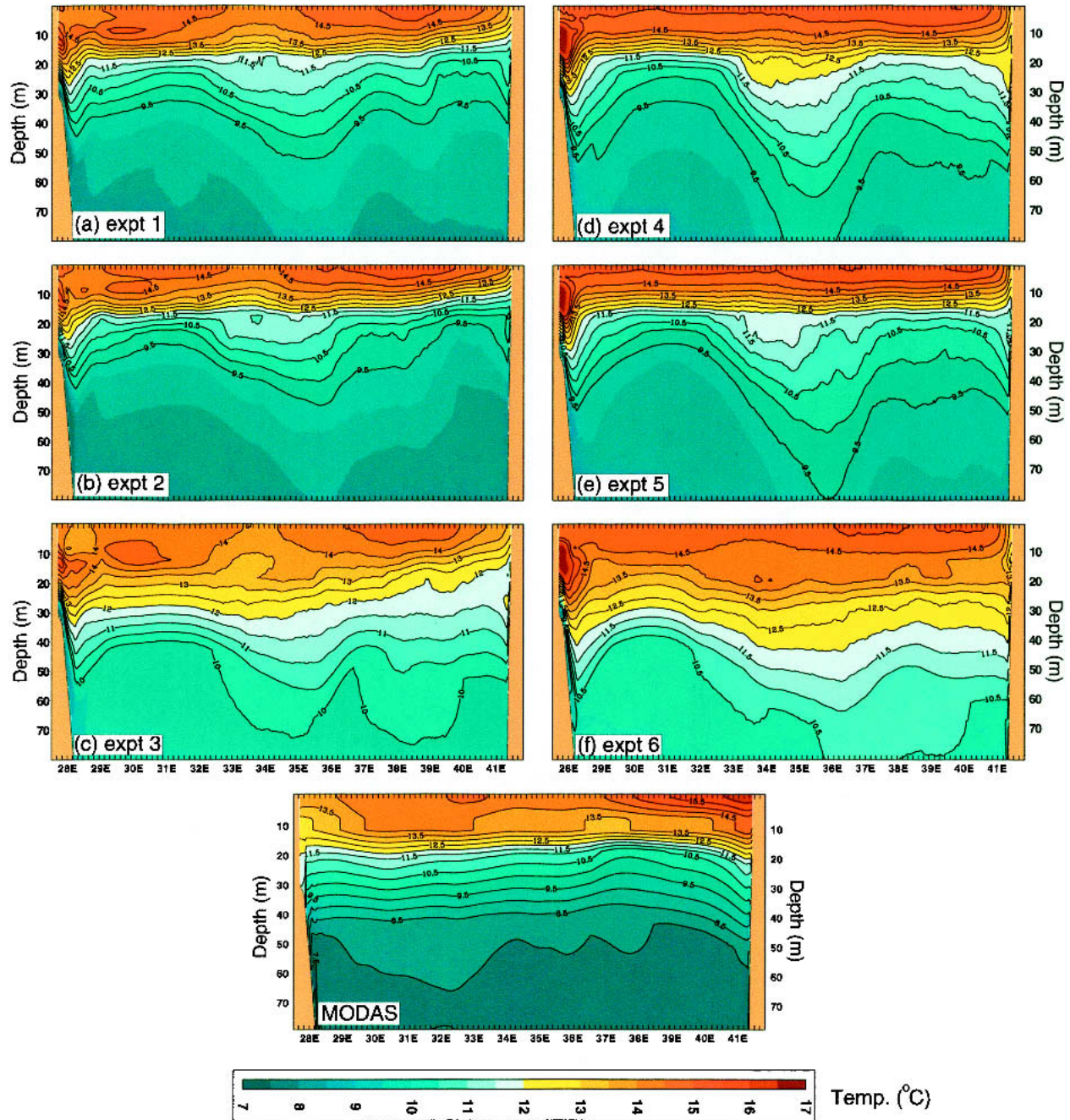


FIG. 9. Black Sea annual mean cross section of temperature along 42.62°N from the surface to 80-m depth. Results from expts 1–6 are seen in (a)–(f), respectively. The annual mean cross section of MODAS subsurface temperatures is also shown for model–data comparison purposes. The climatological annual mean was formed using model years 5–8. It is seen that the Sinop eddy (at around 35.5°E) does not exist in the smooth MODAS climatology. However, standard HYCOM simulations (expts 1 and 4) using SeaWiFS-based monthly turbidity climatology produce the eddy as is consistent with observational studies (e.g., Oguz and Besiktepe 1999; Afanasyev et al. 2002).

tenuation depths from remotely sensed data, 2) implement this scheme into the Hybrid Coordinate Ocean Model, 3) use HYCOM with this solar radiation penetration scheme to model the Black Sea at $\approx 3.2\text{-km}$ resolution, and 4) use the model simulations to ex-

amine the impact of subsurface heating and atmospheric forcing on the upper-ocean circulation structure. To help to assess the robustness of the results, two sets of forcing are used, one from the European Centre for Medium-Range Weather Forecasts reanalysis

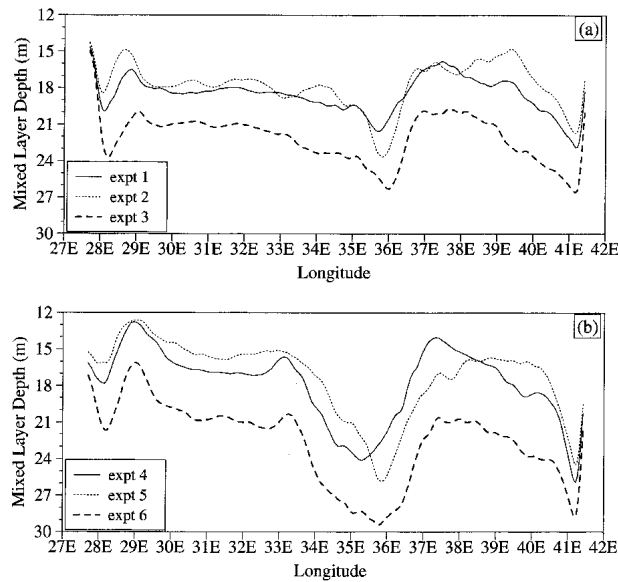


FIG. 10. The annual mean MLD calculated along 42.62°N latitude in the Black Sea: (a) expts 1, 2, and 3 when the HYCOM was run with ECMWF wind/thermal forcing; and (b) expts 4, 5, and 6 when the HYCOM was run with NOGAPS wind/thermal forcing.

(ERA-15), the other from the Fleet Numerical Meteorology and Oceanography Center Navy Operational Global Atmospheric Prediction System data. The model simulations do not include assimilation of any ocean data, except for initialization from climatology and relaxation to bimonthly climatological surface salinity. The hybrid vertical coordinate in HYCOM has isopycnal coordinates in the stratified interior but makes a dynamically smooth transition to depth coordinates in the unstratified mixed layer and terrain-following (σ) coordinates in shallow water. The optimal coordinate for each grid point and each layer is chosen at every time step using the layered continuity equation and a hybrid coordinate generator.

The solar radiation penetration scheme presented in this paper treats attenuation as a continuous quantity and is applicable to any OGCM that has fine vertical resolution near the surface. The climatological monthly mean k_{PAR} fields used in the parameterization of the solar radiation penetration are derived from the remotely sensed Sea-Viewing Wide Field-of-View Sensor data over 1997–2001. These fields provide the first complete datasets of subsurface optical properties that can be used for Black Sea model applications to subsurface heating and bio-optical processes.

The HYCOM simulations from both atmospheric forcing sets demonstrate that assuming all shortwave radiation is absorbed at the surface yields annual mean sea surface currents that are similar to those simulated using spatial and temporal turbidity fields on climatological time scales. A single Jerlov class cannot be used

for any model that includes both the Black Sea and any other sea (e.g., Atlantic or global ocean). This result means that a basin-scale model that would typically use clear water (Jerlov IA) will not perform well in predicting Black Sea upper-ocean quantities, such as sea surface currents and mixed layer depth. The climatological annual mean results discussed here indicate that any ocean model study of the Black Sea circulation needs to use either all shortwave radiation absorbed at the surface or a realistic turbidity via attenuation depths from remotely sensed data (e.g., SeaWiFS). The results also clearly suggest that if the Black Sea turbidity is entirely or largely due to biology, a lack of nutrients (or another cause for a loss of biomass) will have a significant impact on the overall Black Sea circulation. However, a specific examination of the Black Sea ecosystem robustness is not made here. Results presented also reveal that the direct effect of including space–time varying attenuation depths in the Black Sea is a shallowing of the MLD. This shallowing occurs because the heat is not deposited below the MLD in contrast to the clear water constant attenuation depth simulation. Using the clear water attenuation depth of 17 m increases the heating below the mixed layer and weakens the stratification at the base of the mixed layer. This allows the mixed layer to deepen. As a result, changes in the surface currents also occur, such as a weaker mean eddy off Sinop (at around 42.5°N, 35.5°E), regardless of the atmospheric forcing product. In addition, pronounced changes occur in the easternmost Black Sea (e.g., off Trabzon).

The focus of this paper has been on the sensitivity of annual mean upper-ocean quantities (sea surface currents, sea surface height, and MLD) to subsurface heating in the Black Sea. Monthly mean SST predictions from HYCOM in the Black Sea, including extensive model–data comparisons are discussed in Kara et al. (2005b). Monthly analyses of sea surface circulation are addressed in Kara et al. (2005a). The Black Sea model is part of an ongoing global HYCOM development effort and will be a component of the resulting global ocean prediction system, which is planned for operational use at the Naval Oceanographic Office at Stennis Space Center, Mississippi.

Acknowledgments. We extend our special thanks to E. J. Metzger of the Naval Research Laboratory (NRL) at the Stennis Space Center for processing and providing surface forcing fields for the model runs. Numerous discussions with Rainer Bleck from the Atmospheric and Climate Science Department at the Center for Nonlinear Studies (CNLS) of the Los Alamos National Laboratory (LANL) and Eric Chassignet and George Halliwell at the University of Miami Rosenstiel School of Marine and Atmospheric Science (RSMAS) during HYCOM development are greatly appreciated. The reviewers made constructive comments that improved the

quality of this paper. The ocean color data were obtained from the Goddard Distributed Active Archive Center under the auspices of the National Aeronautics and Space Administration (NASA). This dataset is used in accord with the Sea-Viewing Wide Field-of-View Sensor (SeaWiFS) Research Data Use Terms and Conditions Agreement. The numerical HYCOM simulations were performed under the Department of Defense High Performance Computing Modernization Program on an IBM SP POWER3 at the Naval Oceanographic Office, Stennis Space Center, Mississippi, and on an HP/COMPAQ SC45 at the U.S. Army Engineer Research and Development Center (ERDC), Vicksburg, Mississippi. This work is a contribution of the 6.2 Hybrid Coordinate Ocean Model and advanced data assimilation, the NOPP HYCOM consortium for data-assimilative ocean modeling, and the 6.1 Thermodynamic and Topographic Forcing of Global Ocean Models projects. Funding was provided by the Office of Naval Research (ONR) under program elements 602435N for 6.2 and 601153N for 6.1 projects.

REFERENCES

- Afanasyev, Y. D., A. G. Kostianoy, A. G. Zatsepin, and P.-M. Poulain, 2002: Analysis of velocity field in the eastern Black Sea from satellite data during the Black Sea '99 experiment. *J. Geophys. Res.*, **107**, 3098, doi:10.1029/2000JC000578.
- Altman, E. N., and N. I. Kumish, 1986: Interannual and seasonal variability of the Black Sea fresh water balance (in Russian). *Tr. Gos. Okeanogr. Inst.*, **145**, 3–15.
- , I. F. Gertman, and Z. A. Golubeva, 1987: Climatological fields of salinity and temperature in the Black Sea (in Russian). State Oceanographic Institution Tech. Rep., 109 pp. [Available from 2 Kapitanskaya St., Sevastopol 99011, Ukraine.]
- Austin, R. W., and T. J. Petzold, 1986: Spectral dependence of the diffuse attenuation coefficient of light in ocean waters. *Opt. Eng.*, **25**, 471–479.
- Bleck, R., 2002: An oceanic general circulation model framed in hybrid isopycnic-cartesian coordinates. *Ocean Modell.*, **4**, 55–88.
- , and L. Smith, 1990: A wind-driven isopycnic coordinate model of the north and equatorial Atlantic Ocean. 1. Model development and supporting experiments. *J. Geophys. Res.*, **95**, 3273–3285.
- Chassignet, E. P., L. T. Smith Jr., G. R. Halliwell Jr., and R. Bleck, 2003: North Atlantic simulations with the Hybrid Coordinate Ocean Model (HYCOM): Impact of the vertical coordinate choice, reference pressure, and thermobaricity. *J. Phys. Oceanogr.*, **33**, 2504–2526.
- Conkright, M. E., R. A. Locarnini, H. E. Garcia, T. D. O'Brien, T. P. Boyer, C. Stephens, and J. I. Antonov, 2002: *World Ocean Atlas 2001: Objective Analyses, Data Statistics, and Figures, CD-ROM Documentation*. National Oceanographic Data Center, 17 pp.
- Daley, R., 1991: *Atmospheric Data Analysis*. Cambridge University Press, 457 pp.
- Fox, D. N., W. J. Teague, C. N. Barron, M. R. Carnes, and C. M. Lee, 2002: The Modular Ocean Data Assimilation System (MODAS). *J. Atmos. Oceanic Technol.*, **19**, 240–252.
- Gibson, J. K., P. Källberg, S. Uppala, A. Hernandez, A. Nomura, and E. Serrano, 1999: ERA-15 description (version 2). ECMWF Re-Analysis Project Rep. Series 1, 74 pp. [Available from ECMWF, Shinfield Park, Reading RG2 9AX, United Kingdom.]
- Gildor, H., A. H. Sobel, M. A. Cane, and R. N. Sambrotto, 2003: A role for ocean biota in tropical intraseasonal atmospheric variability. *Geophys. Res. Lett.*, **30**, 1460, doi:10.1029/2002GL016759.
- Halliwell, G. R., Jr., 2004: Evaluation of vertical coordinate and vertical mixing algorithms in the HYbrid Coordinate Ocean Model (HYCOM). *Ocean Modell.*, **7**, 285–322.
- Harding, J. M., M. R. Carnes, R. H. Preller, and R. Rhodes, 1999: The Naval Research Laboratory role in naval ocean prediction. *Mar. Technol. Soc. J.*, **33**, 67–79.
- Jerlov, N. G., 1976: *Marine Optics*. Elsevier Oceanography Series, Vol. 14, Elsevier, 231 pp.
- Kara, A. B., P. A. Rochford, and H. E. Hurlburt, 2000: An optimal definition for ocean mixed layer depth. *J. Geophys. Res.*, **105**, 16 803–16 821.
- , —, and —, 2002: Air-sea flux estimates and the 1997–1998 ENSO event. *Bound.-Layer Meteor.*, **103**, 439–458.
- , A. J. Wallcraft, and H. E. Hurlburt, 2003: Climatological SST and MLD simulations from NLOM with an embedded mixed layer. *J. Atmos. Oceanic Technol.*, **20**, 1616–1632.
- , H. E. Hurlburt, P. A. Rochford, and J. J. O'Brien, 2004: The impact of water turbidity on the interannual sea surface temperature simulations in a layered global ocean model. *J. Phys. Oceanogr.*, **34**, 345–359.
- , A. J. Wallcraft, and H. E. Hurlburt, 2005a: How does solar attenuation depth affect the ocean mixed layer? Water turbidity and atmospheric forcing impacts on the simulation of seasonal mixed layer variability in the turbid Black Sea. *J. Climate*, **18**, 389–409.
- , —, and —, 2005b: Sea surface temperature sensitivity to water turbidity from simulations of the turbid Black Sea using HYCOM. *J. Phys. Oceanogr.*, **35**, 33–54.
- Kideys, A. E., A. V. Kovalev, G. Shulman, A. Gordina, and F. Bingel, 2000: A review of zooplankton investigations of the Black Sea over the last decade. *J. Mar. Syst.*, **24**, 355–371.
- Konovalov, S. K., and J. W. Murray, 2001: Variations in the chemistry of the Black Sea on a time scale of decades (1960–1995). *J. Mar. Syst.*, **31**, 217–243.
- Kourafalou, V. H., and E. V. Stanev, 2001: Modeling the impact of atmospheric and terrestrial inputs on the Black Sea coastal dynamics. *Ann. Geophys.*, **19**, 245–256.
- Lalli, C. M., and T. R. Parsons, 1997: *Biological Oceanography: An Introduction*. Butterworth-Heinemann, 314 pp.
- Large, W. G., J. C. McWilliams, and S. C. Doney, 1994: Oceanic vertical mixing: A review and a model with a nonlocal boundary layer parameterization. *Rev. Geophys.*, **32**, 363–403.
- , G. Danabasoglu, S. C. Doney, and J. C. McWilliams, 1997: Sensitivity to surface forcing and boundary layer mixing in a global ocean model: Annual mean climatology. *J. Phys. Oceanogr.*, **27**, 2418–2447.
- Laws, E. A., G. R. DiTullio, K. L. Carder, P. R. Betzer, and S. Hawes, 1990: Primary production in the deep blue sea. *Deep-Sea Res.*, **37**, 715–730.
- Leveque, R. J., 2002: *Finite Volume Methods for Hyperbolic Problems*. Cambridge University Press, 578 pp.
- Levitus, S., and T. P. Boyer, 1994: *Temperature*. Vol. 4, *World Ocean Atlas 1994*, NOAA Atlas NESDIS 4, 117 pp.
- , R. Burgett, and T. P. Boyer, 1994: *Salinity*. Vol. 3, *World Ocean Atlas 1994*, NOAA Atlas NESDIS 3, 99 pp.
- Lewis, M. R., M. E. Carr, G. Feldman, C. R. McClain, and W. Esaias, 1990: Influence of penetrating radiation on the heat budget of the equatorial Pacific Ocean. *Nature*, **347**, 543–545.
- Liu, W. T., A. Zhang, and J. K. B. Bishop, 1994: Evaporation and solar irradiance as regulators of sea surface temperature in annual and interannual changes. *J. Geophys. Res.*, **99**, 12 623–12 637.
- McClain, C. R., M. L. Cleave, G. C. Feldman, W. W. Gregg, S. B.

- Hooker, and N. Kuring, 1998: Science quality SeaWiFS data for global biosphere research. *Sea Technol.*, **39**, 10–16.
- Morel, A., and D. Antonie, 1994: Heating rate within the upper ocean in relation to its bio-optical state. *J. Phys. Oceanogr.*, **24**, 1652–1665.
- , and S. Maritorena, 2001: Bio-optical properties of oceanic waters: A reappraisal. *J. Geophys. Res.*, **106**, 7163–7180.
- Murray, J. W., Z. Top, and E. Ozsoy, 1991: Hydrographic properties and ventilation of the Black Sea. *Deep-Sea Res.*, **38**, 663–690.
- Murtugudde, R., J. Beauchamp, C. R. McClain, M. R. Lewis, and A. J. Busalacchi, 2002: Effects of penetrative radiation on the upper tropical ocean circulation. *J. Climate*, **15**, 470–486.
- Nakamoto, S., P. Kumar, J. M. Oberhuber, J. Ishizaka, K. Muneyama, and R. Frouin, 2001: Response of the equatorial Pacific to chlorophyll pigment in a mixed layer isopycnal ocean general circulation model. *Geophys. Res. Lett.*, **28**, 2021–2024.
- NAVOCEANO, 2003: Database description for the generalized digital environmental model (GDEM-V) Version 3.0. OAML-DBD-72, 34 pp. [Available from Naval Oceanographic Office, Oceanographic Data Bases Division, Stennis Space Center, MS 39522-5001.]
- NOAA, 1988: Digital relief of the surface of the Earth. Data Announcement 88-MGG-02. [Available from NOAA National Geophysical Data Center, E/GC 325 Broadway, Boulder, CO 80305-3328.]
- Oguz, T., and S. Besiktepe, 1999: Observations on the Rim Current structure, CIW formation and transport in the Western Black Sea. *Deep-Sea Res.*, **46A**, 1733–1753.
- , and Coauthors, 1993: Circulation in the surface and intermediate layers of the Black Sea. *Deep-Sea Res.*, **40A**, 1597–1612.
- , P. Malanotte-Rizzoli, H. W. Ducklow, and J. W. Murray, 2002: Interdisciplinary studies integrating the Black Sea biogeochemistry and circulation dynamics. *Oceanography*, **15**, 4–11.
- Ohlmann, J. C., 2003: Ocean radiant heating in climate models. *J. Climate*, **16**, 1337–1351.
- , D. Siegel, and L. Washburn, 1998: Radiant heating of the western equatorial Pacific during TOGA-COARE. *J. Geophys. Res.*, **103**, 5379–5395.
- Ozsoy, E., and U. Unluata, 1997: Oceanography of the Black Sea: A review of some recent results. *Earth-Sci. Rev.*, **42**, 231–272.
- , —, and Z. Top, 1993: The evaluation of Mediterranean water in the Black Sea: Interior mixing and material transport by double diffusive intrusions. *Progress in Oceanography*, Vol. 31, Pergamon, 275–320.
- Paulson, C. A., and J. J. Simpson, 1977: Irradiance measurements in the upper ocean. *J. Phys. Oceanogr.*, **7**, 953–956.
- Perry, G. D., P. B. Duffy, and N. L. Miller, 1996: An extended data set of river discharges for validation of general circulation models. *J. Geophys. Res.*, **101**, 21 339–21 349.
- Rochford, P. A., A. B. Kara, A. J. Wallcraft, and R. A. Arnone, 2001: Importance of solar subsurface heating in ocean general circulation models. *J. Geophys. Res.*, **106**, 30 923–30 938.
- Rosmond, T. E., J. Teixeira, M. Peng, T. F. Hogan, and R. Pauley, 2002: Navy Operational Global Atmospheric Prediction System (NOGAPS): Forcing for ocean models. *Oceanography*, **15**, 99–108.
- Schneider, E. K., and Z. Zhu, 1998: Sensitivity of the simulated annual cycle of sea surface temperature in the equatorial Pacific to sunlight penetration. *J. Climate*, **11**, 1933–1950.
- Schneider, N., T. Barnett, M. Latif, and T. Stockdale, 1996: Warm pool physics in a coupled GCM. *J. Climate*, **9**, 219–239.
- , A. J. Miller, and D. W. Pierce, 2002: Anatomy of North Pacific decadal variability. *J. Climate*, **15**, 586–605.
- Siegel, D. A., J. C. Ohlmann, L. Washburn, R. Bidigare, C. Nosse, E. Fields, and Y. Zhou, 1995: Solar radiation, phytoplankton pigments and radiant heating of the equatorial Pacific. *J. Geophys. Res.*, **100**, 4885–4891.
- Simonot, J.-Y., and H. Le Treut, 1986: A climatological field of mean optical properties of the world ocean. *J. Geophys. Res.*, **91**, 6642–6646.
- Smagorinsky, J. S., 1963: General circulation experiments with the primitive equations. I: The basic experiment. *Mon. Wea. Rev.*, **91**, 99–164.
- Smyth, W. D., E. D. Skyllingstad, G. Crawford, and H. Wijesekera, 2002: Nonlocal fluxes and Stokes drift effects in the K-Profile Parameterization. *Ocean Dyn.*, **52**, 104–115.
- Sorkina, A. I., 1974: *Reference Book on the Black Sea Climate* (in Russian). Gidrometeoizdat, 406 pp.
- Stanev, E. V., 1990: On the mechanisms of the Black Sea circulation. *Earth-Sci. Rev.*, **28**, 285–319.
- , and J. M. Beckers, 1999: Barotropic and baroclinic oscillations in strongly stratified ocean basins: Numerical study of the Black Sea. *J. Mar. Syst.*, **19**, 65–112.
- , and J. V. Staneva, 2000: The impact of the baroclinic eddies and basin oscillations on the transitions between different quasi-stable states of the Black Sea circulation. *J. Mar. Syst.*, **24**, 3–26.
- , and —, 2001: The sensitivity of the heat exchange at sea surface to meso and sub-basin scale eddies: Model study for the Black Sea. *Dyn. Atmos. Oceans*, **33**, 163–189.
- Staneva, J. V., and E. V. Stanev, 1998: Oceanic response to atmospheric forcing derived from different climate data sets. *Oceanol. Acta*, **21**, 393–417.
- , D. E. Dietrich, E. V. Stanev, and M. J. Bowman, 2001: Rim Current and coastal eddy mechanisms in an eddy-resolving Black Sea general circulation model. *J. Mar. Syst.*, **31**, 137–157.
- Sur, H. I., and Y. P. Ilyin, 1997: Evolution of satellite derived mesoscale thermal patterns in the Black Sea. *Progress in Oceanography*, Vol. 39, Pergamon, 109–151.
- , E. Ozsoy, Y. P. Ilyin, and U. Unluata, 1996: Coastal/deep ocean interactions in the Black Sea and their ecological/environmental impacts. *J. Mar. Syst.*, **7**, 293–320.
- van Leer, B., 1977: Towards the ultimate conservative difference scheme IV. A new approach to numerical convection. *J. Comput. Phys.*, **23**, 276–299.
- Vörösmarty, C. J., K. Sharma, B. M. Fekete, A. H. Copeland, J. Holden, J. Marble, and J. A. Lough, 1997: The storage and aging of continental runoff in large reservoir systems of the world. *Ambio*, **26**, 210–219.
- , B. M. Fekete, and B. A. Tucker, 1998: River, Discharge Database, (RivDIS) V1.1. Version 1.1. [Available from the Institute for the Study of Earth, Oceans, and Space, University of New Hampshire, 39 College Rd., Durham, NH 03824.]
- Wallcraft, A. J., A. B. Kara, H. E. Hurlburt, and P. A. Rochford, 2003: The NRL Layered Global Ocean Model (NLOM) with an embedded mixed layer submodel: Formulation and tuning. *J. Atmos. Oceanic Technol.*, **20**, 1601–1615.
- Zaneveld, J. R. V., J. C. Kitchen, and J. L. Müeller, 1993: Vertical structure of productivity and its vertical integration as derived from remotely sensed observations. *Limnol. Oceanogr.*, **38**, 1384–1393.